Published OnlineFirst October 21, 2019; DOI: 10.1158/1078-0432.CCR-19-1868

Macrophage-Derived CXCL9 and CXCL10 Are Required for Antitumor Immune Responses Following Immune Checkpoint Blockade

Imran G. House[1,2], Peter Savas[2,3], Junyun Lai[1,2], Amanda X.Y. Chen[1,2], Amanda J. Oliver[1,2], Zhi L. Teo[2,3], Kirsten L. Todd[1,2], Melissa A. Henderson[1,2], Lauren Giuffrida[1,2], Emma V. Petley[1,2], Kevin Sek[1,2], Sherly Mardiana[1,2], Tuba N. Gide[4], Camelia Quek[4], Richard A. Scolyer[4,5], Georgina V. Long[4,6,7], James S. Wilmott[4], Sherene Loi[2,3], Phillip K. Darcy[1,2,8,9], and Paul A. Beavis[1,2]

ABSTRACT

Purpose: Response rates to immune checkpoint blockade (ICB; anti-PD-1/anti-CTLA-4) correlate with the extent of tumor immune infiltrate, but the mechanisms underlying the recruitment of T cells following therapy are poorly characterized. A greater understanding of these processes may see the development of therapeutic interventions that enhance T-cell recruitment and, consequently, improved patient outcomes. We therefore investigated the chemokines essential for immune cell recruitment and subsequent therapeutic efficacy of these immunotherapies.

Experimental Design: The chemokines upregulated by dual PD-1/CTLA-4 blockade were assessed using NanoString-based analysis with results confirmed at the protein level by flow cytometry and cytometric bead array. Blocking/neutralizing antibodies confirmed the requirement for key chemokines/cytokines and immune effector cells. Results were confirmed in patients treated with immune checkpoint inhibitors using single-cell RNA-sequencing (RNA-seq) and paired survival analyses.

Results: The CXCR3 ligands, CXCL9 and CXCL10, were significantly upregulated following dual PD-1/CTLA-4 blockade and both $CD8^+$ T-cell infiltration and therapeutic efficacy were CXCR3 dependent. In both murine models and patients undergoing immunotherapy, macrophages were the predominant source of CXCL9 and their depletion abrogated $CD8^+$ T-cell infiltration and the therapeutic efficacy of dual ICB. Single-cell RNA-seq analysis of patient tumor-infiltrating lymphocytes (TIL) revealed that CXCL9/10/11 was predominantly expressed by macrophages following ICB and we identified a distinct macrophage signature that was associated with positive responses to ICB.

Conclusions: These data underline the fundamental importance of macrophage-derived CXCR3 ligands for the therapeutic efficacy of ICB and highlight the potential of manipulating this axis to enhance patient responses.

Introduction

Immunotherapy, and in particular immune checkpoint therapy, has emerged as a powerful treatment strategy in several cancer types (1). Immune checkpoint inhibitors such as anti-PD-1, anti-PD-L1, and anti-CTLA-4 used alone or in combination provide durable responses in a subset of patients. However, it is not fully understood which parameters influence the likelihood of patient response (1, 2). Factors that have been reported to predict responses to immune checkpoint inhibitors include the mutational load of the tumor (3), the expression of target ligands such as PD-L1, and the presence of high number of TILs (4). It is now clear that the number of $CD8^+$ T cells at the tumor site is a strong predictor of response to anti-PD-1 therapy in melanoma (4). However, a large proportion of patients exhibit an immune-exclusion or immune-desert phenotype and a number of strategies are currently being developed to enhance immune infiltrate in this patient subtype (5). The efficacy of immune checkpoint blockade depends upon the recruitment of tumor-infiltrating lymphocytes and yet the mechanism by which this occurs is largely unknown. Because the trafficking of immune cells, including T cells, is modulated by chemokine:chemokine receptor interactions, this prompted us to evaluate the chemokine networks responsible for the recruitment of T cells following immune checkpoint blockade. Chemokines interact with their respective chemokine receptors and this binding leads to the activation of intracellular signaling pathways that result in the migration of the target cells toward the source of the chemokine. T cells express a range of chemokine receptors including CCR2, CCR4, CCR5, and CXCR3, which respond to a range of chemokines. In the context of cancer, the ligands of CCR5 (CCL5) and CXCR3 (CXCL9, CXCL10, and CXCL11) have been shown to associate with levels of TIL infiltrate in human cancers (6–8) and the production of CXCL9 and CXCL10 has been associated with improved responses to chemotherapy (9–11) and adoptive

[1]Cancer Immunology Program, Peter MacCallum Cancer Centre, Melbourne, Victoria, Australia. [2]Sir Peter MacCallum Department of Oncology, The University of Melbourne, Parkville, Australia. [3]Division of Research, Peter MacCallum Cancer Centre, University of Melbourne, Melbourne, Victoria, Australia. [4]The University of Sydney, Melanoma Institute Australia, Sydney, New South Wales, Australia. [5]Royal Prince Alfred Hospital, Sydney, New South Wales, Australia. [6]Royal North Shore Hospital, Sydney, New South Wales, Australia. [7]Mater Hospital, North Sydney, New South Wales, Australia. [8]Department of Pathology, University of Melbourne, Parkville, Victoria, Australia. [9]Department of Immunology, Monash University, Clayton, Victoria, Australia.

Note: Supplementary data for this article are available at Clinical Cancer Research Online (http://clincancerres.aacrjournals.org/).

I.G. House and P. Savas contributed equally to this article.

P.K. Darcy and P.A. Beavis are the co-senior authors of this article.

Corresponding Authors: Paul A. Beavis, Peter MacCallum Cancer Research Centre, Melbourne, Victoria, Australia. E-mail: paul.beavis@petermac.org; and Phillip K. Darcy, phil.darcy@petermac.org

Clin Cancer Res 2020;26:487–504

doi: 10.1158/1078-0432.CCR-19-1868

Published OnlineFirst October 21, 2019; DOI: 10.1158/1078-0432.CCR-19-1868

Translational Relevance

Treatment with immune checkpoint inhibitors has been highly successful in a subset of tumor types, particularly those with increased levels of immune infiltrate. However, the mechanism and the immune cell subsets critical for successful clinical responses are not fully understood. This study demonstrates that the chemokines CXCL9/10 are indispensable for robust responses to immune checkpoint inhibitors (anti-PD-1 and anti-CTLA-4) and, in particular, that CXCL9/10-secreting macrophages are critical for their therapeutic efficacy. Moreover, we identified a novel transcriptional signature in macrophages that was associated with positive patient responses to immune checkpoint inhibitors that was lacking in nonresponding patients. This is of significant interest to the field, challenging the paradigm that macrophages are protumoral and detrimental to antitumor immune responses through immunosuppressive mechanisms, including expression of PD-L1. These findings indicate that the intratumoral macrophage phenotype is a key feature in determining responses to immune checkpoint inhibitors that can be exploited either diagnostically or therapeutically.

cellular therapy (12–14). CXCL11 binds to CXCR3 with the highest affinity, followed by CXCL10 and CXCL9 (15, 16) and notably CXCL11 binds to the CXCR3 receptor at a distinct binding site of the receptor (17), potentially leading to diverse signaling outcomes (18).

In this study, an unbiased analysis of the maximally upregulated chemokines following dual PD-1/CTLA-4 blockade revealed that CXCL9 and CXCL10 were significantly upregulated in the tumor microenvironment following therapy. Neutralization of CXCR3, the receptor for CXCL9 and CXCL10, abrogated the therapeutic efficacy of dual PD-1/CTLA-4 blockade and was associated with reduced infiltration and activation phenotype of $CD8^+$ T cells in the tumor and draining lymph nodes. This induction of CXCL9 was dependent on the production of IFNγ because blockade of this cytokine reduced the production of CXCL9 following therapeutic intervention. CRISPR-Cas9–mediated knockout of CXCL9/10 in tumor cells revealed that production of these chemokines by the tumor cells was not required for the efficacy of immune checkpoint blockade, inferring an important role for host-derived chemokines. Interrogation of the source of CXCL9 revealed that macrophages were a major source of CXCL9 chemokine and that depletion of these cells significantly impaired the efficacy of dual PD-1/CTLA-4 blockade. Furthermore, investigation of the relevance of this axis in patients treated with either atezolizumab (anti-PD-L1) or nivolumab (anti-PD-1), respectively, revealed that the production of CXCL9 and CXCL10 was highly associated with improved patient prognosis and correlated with an IFN signature, underlining the importance of IFNγ in mediating this effect. Notably, single-cell analysis of patient tumors confirmed that macrophages were a major source of CXCL9 both prior to and after immune checkpoint blockade. These studies reveal the critical importance of CXCL9 induction postimmunotherapy, allowing for the effective trafficking and activation of T cells. This suggests that enhancing CXCL9 production by macrophages could be an effective therapeutic strategy to enhance the efficacy of immunotherapy, particularly in patients with low levels of immune cells.

Materials and Methods

Cell lines and mice

The C57BL/6 mouse breast carcinoma cell line AT-3, was obtained from Dr. Trina Stewart (Griffith University, Queensland, Australia) and transduced to express chicken ovalbumin as described previously ($AT\text{-}3ova^{dim}$; ref. 19). B16F10-ova tumor cells were obtained from Dr. Jason Waithman (Telethon Kid's Institute, Nedlands, Western Australia), MC38 tumor cells were obtained from Dr. Nicole Haynes (Peter MacCallum Cancer Centre, Melbourne, Victoria, Australia) and E0771 tumor cells were obtained from Prof. Robin Anderson (Olivia Newton-John Cancer Research Institute, Victoria, Australia). Tumor lines were verified to be *Mycoplasma* negative by PCR analysis and were actively passaged for less than 6 months. Tumor cells were grown in DMEM supplemented with 10% FCS, Glutamax, and penicillin/streptomycin. For *in vivo* experiments, the indicated number of cells were resuspended in PBS and injected subcutaneously (100 μL) or into the fourth mammary fat pad (E0771; 20 μL). C57BL/6 WT mice were obtained from the Walter and Eliza Hall Institute of Medical Research (Melbourne, Australia) and $BATF3^{-/-}$ mice were bred in house. All animal experiments were approved by the Animal Experimental Ethics Committee (Peter MaCallum Cancer Centre, Victoria, Australia; protocol E582).

IHC

Tumors were harvested and fixed overnight in 10 % neutral buffered formalin (NBF). Fixed samples were embedded in paraffin and 4-μm–thick sections were cut onto glass slides. Before staining, samples were dewaxed in xylene and antigens retrieved at 125°C for 3 minutes in 10 mmol/L citrate buffer (Sigma) pH 6. For staining, Perkin Elmer OPAL reagents were used as per kit instructions. Antibodies and fluorophores were used in the following order: CD3 (Abcam SP7, 1:200) 690; FoxP3 (eBioscience FJK-16s, 10 μg/mL) 540; PD-1 (Abcam EPR20665, 0.8 μg/mL) 620; CD8 (eBioscience 4SM15, 5 μg/mL) 570; CK8 (Abcam EP1628Y, 0.2 μg/mL) 520; and DAPI. Multiplexing IHC images were visualized using the Perkin Elmer Vectra 3 microscope and analyzed using InForm v2.4.0 (Perkin Elmer) and HALO v2.3 (Indica labs).

Antibodies and treatment of tumor-bearing mice

Antibodies to PD-1 (RMP1-14), CTLA-4 (9H10), isotype control (2A3), the depleting antibody anti-F4/80 (CI:A3-1), and the neutralizing antibodies for CXCR3 (CXCR3-173), IFNγ (H22), and TNFα (TN3-19.12) were purchased from BioXcell. Mice were treated once every 4 days with either isotype control (2A3), anti-PD-1 (RMPI-14), and/or anti-CTLA-4 (9H10) for up to 4 doses.

Analysis of tumor-infiltrating immune subsets

Seven days posttreatment, tumors were excised and digested postmortem using a cocktail of 1 mg/mL collagenase type IV (Sigma-Aldrich) and 0.02 mg/mL DNAase (Sigma-Aldrich). After digestion at 37°C for 30 minutes, cells were passed through a 70-μm filter twice. Inguinal lymph nodes were also harvested and cells filtered through a 70-μm filter. Cells were then analyzed by flow cytometry as described previously (19) and Fixable Yellow (Thermo Fisher Scientific) used as a viability dye.

Intracellular cytokine staining

For detection of IFNγ and TNFα production by T cells *ex vivo*, TILs cells were cultured for 3 hours with 10 ng/mL PMA and 1 μg/mL ionomycin in the presence of Golgi Plug (BD Pharmingen) and Golgi Stop (BD Pharmingen). After 3 hours, cells were analyzed by flow

Published OnlineFirst October 21, 2019; DOI: 10.1158/1078-0432.CCR-19-1868

cytometry. For the detection of CXCL9, cells were cultured for 3 hours in Golgi Plug/Stop in the absence of PMA/ionomycin.

Cytometric bead array

Analysis of cytokine and chemokine concentrations was performed using either the BioLegend Legendplex kit (#74041) or paired cytometric bead array reagents (BD Biosciences) as per the manufacturer's instructions.

Gene expression analysis

RNA prepared from tumor cells was quantified and quality assessed using Tapestation analysis. Gene count were determined by Peter MacCallum Cancer Centre Advanced Genomica Core by nCounter XT assay (Mouse Pan Cancer Immune Profiling; NanoString Technologies 115000142) and analyzed by nSolver 4.0 software as per the manufacturer's instructions.

Default quality control and normalization steps showed all samples were adequate for further analysis. Differential expression between treatment groups was performed with the R package limma (version 3.36.5; ref. 20), using TMM (21) normalization and transformation of counts with "voom" (22). To create the mean-difference plot, the average expression of each gene was plotted against $\log_2$ of the fold change between groups. Genes with an adjusted *P* value less than 0.05 calculated by the differential expression methodology of limma were highlighted.

Four clinical cohorts were utilized for analysis of the prognostic impact of chemokine expression. Gide and colleagues analyzed a cohort of patients with metastatic melanoma treated with immune checkpoint blockade and classified as responders or nonresponders (23). The cohort consisted of 41 biopsies at baseline and 9 biopsies on-treatment from patients treated with anti-PD1 monotherapy, and 32 biopsies at baseline and 9 biopsies on-treatment from patients treated with combination anti-PD1 and anti-CTLA-4. Bulk RNA-seq and survival data were available for all patients, and 56 patients had IHC quantification of intratumoral CD8 T cells in baseline samples. IMvigor210 was a phase II trial investigating PD-L1 blockade with atezolizumab 1,200 mg 3-weekly in patients with metastatic urothelial carcinoma that had progressed on prior platinum-based chemotherapy. Overall survival data and whole transcriptome RNA-seq was available for 348 cases (24). The METABRIC cohort consists of primary breast cancers that underwent microarray gene expression profiling, and have long-term survival follow up available. Triple-negative cases were selected according to the absence of estrogen receptor staining and absence of HER2 amplification determined by SNP array. Gene expression data are available as log-transformed normalized expression values. The TCGA Melanoma cohort consists of primary melanomas that underwent RNA-seq with the data provided as transcripts per million (TPM). All survival analyses were done with the R package "survival." In each cohort, cases were divided into two groups: cases where expression of the gene in question was above the median, and cases where gene expression was equal to or below the median. The overall survival function of each group was estimated with the Kaplan–Meier method and compared using the log-rank test. Survival curve plots were generated with the R package "survminer."

Bulk RNA-seq

Differential expression results between tumors from responders and nonresponders was obtained from the R package "IMvigor210CoreBiologies" associated with the original publication (24) and available at http://research-pub.gene.com/IMvigor210CoreBiologies/. No modifications to the published differential expression analysis were made. In a second analysis of gene sets associated with CXCL9 and CXCL10 expression, the IMvigor cohort was reanalyzed from raw count data. The count matrix was filtered to remove unexpressed genes followed by principal component analysis (PCA) to identify outlier samples that were excluded. Counts were transformed to counts per million and samples were ranked by CXCL9 or CXCL10 expression and split into two groups above and below the median expression. Competitive gene set testing between high and low expression groups was performed with limma's "camera" function (25), using Reactome gene sets from the Molecular Signatures Database version 5.6 C2 collection and GO term associated gene sets from the C5 collection (26). Enrichment barcode plots were generated with a modified version of limma's "barcodeplot" function. Log_{10} transformed gene counts per million were used for correlations and survival analyses with the cohort split by median gene expression as described. The Gide and colleagues melanoma dataset described in the previous section was analyzed as per the original study, with $\log_{10}$ transformed counts per million used for correlations and survival analyses (23). Data from another cohort of patients with metastatic melanoma treated with checkpoint blockade associated with Riaz and colleagues (27) were obtained from https://github.com/riazn/bms038_analysis/. Differential expression between baseline and on-treatment biopsies was performed with limma, using the duplicate Correlation function for repeat biopsy samples. Adjusted *P* values were calculated according to the method of Benjamini and Hochberg. A CTC score was calculated per sample from the mean of $\log_{10}$-transformed gene expression values for CD8A, CD8B, GZMA, GZMB, and PRF1 (28).

Single-cell mRNASeq datasets

Four independent cohorts of single-cell mRNASeq on immune infiltrates from human tumors were analyzed: metastatic melanoma studies by Sade-Feldman and colleagues (29) and Jerby-Arnon and colleagues (30), head and neck carcinoma study by Puram and colleagues (31); lung carcinoma study by Zilionis and colleagues (32). See the associated publications for further details and data availability. The Sade-Feldman dataset also contains clinical information and outcome after treatment with checkpoint blockade. The R package Seurat (version 3.0) was used to analyze these datasets (33). Raw data consisted of gene expression values in TPM. $\text{Log}_2(\text{TPM}/10 + 1)$ was used for downstream analysis (30). For each dataset, variable genes were selected prior to dimensionality reduction with PCA. Significant principal components were selected with Seurat JackStraw permutation testing. These components were supplied to the UMAP algorithm (https://arxiv.org/abs/1802.03426) to generate a two-dimensional projection for visualization purposes. The head and neck data from Puram and colleagues displayed batch effects related to different sample preparation methods. This effect was corrected using the data integration method of Seurat. No batch effects were seen related to known experimental factors in the other studies. For each dataset, the cluster assignments determined in the original publications were maintained. All single-cell plots were generated using log-transformed TPM/10 values. Differential expression between groups of cells was performed using MAST (34), and P_{adj} values calculated with the Bonferroni correction. In the Sade-Feldman and colleagues' dataset, cases were classified in various ways regarding response, by response of the lesion that was biopsied and the overall clinical response. The latter was used in classifying a case as a responder or nonresponder. Two cases were classified as treatment resistance, as they develop progressive

Published OnlineFirst October 21, 2019; DOI: 10.1158/1078-0432.CCR-19-1868

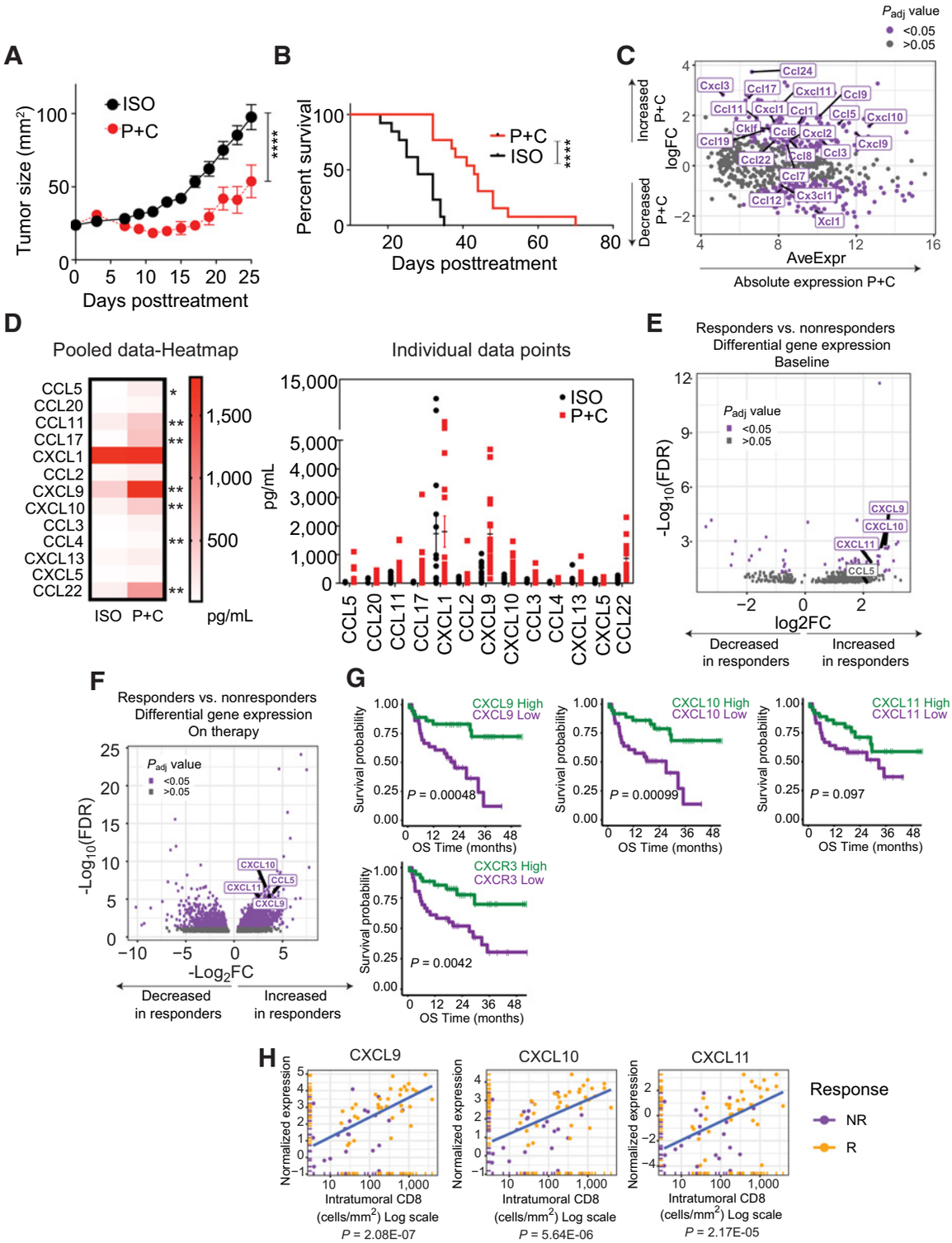

Figure 1.

CXCL9 and CXCL10 are upregulated upon dual PD-1 and CTLA-4 blockade and correlate with survival in patient cohorts treated with immune checkpoint blockade. **A,** C57BL/6 mice were injected subcutaneously with 5×10^5 AT-3ova cells and allowed to establish for 14 days, following which they were treated on days 14, 18, 22, and 26 with either dual treatment with anti-PD-1 (200 μg/mouse) and anti-CTLA-4 (150 μg/mouse; P+C) or isotype control (ISO; 200 μg/mouse). Data shown as the mean ± SEM of 6–8 mice per group of a representative experiment ($n > 3$). (*Continued on the following page.*)

Published OnlineFirst October 21, 2019; DOI: 10.1158/1078-0432.CCR-19-1868

disease after an initial brief response. These cases were excluded to provide more distinct biology for comparison of responders and nonresponders. A gene signature was created from differential expression results by selecting genes with an $P_{adj} < 0.05$ and $\log_2$ fold change > 2. The per cell signature score was calculated by the sum of the expression of upregulated signature genes minus the expression of downregulated signature genes, using scaled data in Seurat.

Single-cell mRNASeq from the CT26 melanoma syngeneic model was also analyzed in a similar fashion to the above (35). As this data is unique molecular identifier based, the sctransform normalization and variance stabilization method was used.

Data availability

NanoString data generated in this study is included as a Supplementary File.

METABRIC-processed gene expression data is available at www.cbioportal.org and clinical data are available as Supplementary Table S1 in Rueda and colleagues' study (36).

The Cancer Genome Atlas (TCGA) melanoma gene expression data is available at www.cbioportal.org under the TCGA pan-cancer atlas 2018 dataset, and curated survival data was obtained from Supplementary Table S1 in Liu and colleagues (37).

IMvigor210 data can be found in the R package at http://research-pub.gene.com/IMvigor210CoreBiologies/.

Riaz and colleagues' metastatic melanoma data is available at https://github.com/riazn/bms038_analysis/tree/master/data.

Gide and colleagues' metastatic melanoma data is available in the European Nucleotide Archive under accession PRJEB23709.

Single-cell mRNASeq data are available from the Gene Expression Omnibus; Sade-Feldman and colleagues' melanoma single-cell data under accession number GSE120575, Jerby-Arnon and colleagues' melanoma single-cell data under accession number GSE115978; Puram and colleagues' head and neck data under GSE103322; Zilionis and colleagues' lung cancer data GSE127465; and Kumar and 'colleagues CT26 syngeneic model data GSE121861.

Quantitative real-time PCR analysis

RNA was isolated using an RNeasy Mini Kit (Qiagen) following which cDNA was generated using M-MLV Reverse Transcriptase (Promega) as per the manufacturers' instructions. qRT-PCRs were performed using SensiFAST SYBR (Bioline) and performed on StepOnePlus (Applied Biosystems). The following primers were used: CXCL9 forward (F): 5′- ATCTTCCTGGAGCAGTGTGG-3′, reverse (R): 5′-AGTCCGGATCTAGGCAGGTT-3′; CXCL10 F: 5′-GTGAGAATGAGGGCCATAGG-3′, R: 5′-GGCTAAACGCTTTCATTAAATTC-3′: CXCR3 F: 5′-GCCAAGCCATGTACCTTGAG-3′, R: 5′-TCAGGCTGAAATCCTGTGG-3′; GAPDH F: 5′- AACTTTGGCATTGTGGAAGG-3′, R: 5′-GGATGCAGGGATGATGTTCT-3′; RPL27 F: 5′- AAGCCGTCATCGTGAAGAACA-3′, R: 5′- CTTGATCTTGGATCGCTTGGC-3′.

Western immunoblotting

Protein lysates were generated in 1% NP40 lysis buffer and boiled and resolved in Laemmli buffer in reducing conditions using 10% acrylamide SDS-PAGE. Protein was then transferred to polyvinylidene difluoride membrane (Millipore) and probed with antibodies for CXCL9 (R&D Systems) and CXCL10 (R&D Systems) and secondary antibodies conjugated with horseradish peroxidase. X-ray film was used to detect chemiluminescence.

CRISPR knockout cell line generation

To generate knockout cell lines, 37 pmoles sgRNA (Synthego) and 270 pmoles recombinant Cas9 (IDT) were incubated together for 10 minutes at room temperature. sgRNA/Cas9 RNPs were then electroporated into AT-3ova cells (3×10^5) using a Lonza SG Cell line kit and 4D-Nucleofector. Gene knockout was confirmed 48 hours later by Western immunoblot analysis. Two sgRNAs were used per gene. Sequences used were as follows: CXCL9 g1:auuuguaguggaucgugccu and g2: aaccugccuagauccggacu; CXCL10 g1:ugacgggccagugagaauga and g2: ugagcagagaugucugaauc.

Statistical analysis

Statistical differences were analyzed by one-way ANOVA, two-way ANOVA, or unpaired *t* test, where appropriate, as stated in text. $P < 0.05$ was considered significant.

Results

Intratumoral CXCL9 and CXCL10 expression is increased following immune checkpoint blockade

To investigate the chemokines required for effective therapeutic responses following immune checkpoint blockade we utilized the AT-3ova model of triple-negative breast cancer, which we have previously shown to be responsive to dual PD-1/CTLA-4 blockade (19). As expected, when mice bearing AT-3ova tumors were treated with anti-PD-1 and anti-CTLA-4 at day 14 post tumor inoculation, robust antitumor immune responses were observed (**Fig. 1A** and **B**), while single-agent treatment with either anti-PD-1 or anti-CTLA-4 resulted in limited antitumor activity (Supplementary Fig. S1A). Because treatment of tumors with anti-PD-1/anti-CTLA-4 is known to be associated with an increase in tumor-infiltrating lymphocytes (19, 38), we investigated the chemokines that were upregulated in this context by performing gene expression analysis on tumor samples obtained from mice treated with 2A3 isotype control or anti-PD-1 and anti-CTLA-4. This analysis revealed significant upregulation of numerous cytokines and chemokines associated with T-cell infiltration with CXCL9 ($P = 0.001$) and CXCL10 ($P = 0.0001$) being two of the most significantly upregulated and abundant chemokines following dual immune checkpoint blockade (**Fig. 1C**). Similarly, CXCR3, the receptor for CXCL9/CXCL10, was also significantly upregulated in tumors treated with

(*Continued.*) **B,** Mouse survival is shown as combined data of two independent experiments. ****, $P < 0.0001$ (determined by two-way ANOVA and Mantel–Cox test). **C** and **D,** Seven days posttreatment, tumors were harvested ($n = 3$ per group) and gene expression was analyzed by NanoString and presented as an MA plot (**C**). **D,** Tumors were cultured in PBS for 4 hours at 37°C (2 μL per mg of tissue) and chemokine expression determined by cytometric bead array. *, $P < 0.05$; **, $P < 0.005$; multiple *t* test. $N = 18$–19 mice per group. **E–H,** Analysis of patient datasets as described in ref. 23. Differential gene expression analysis comparing responders ($n = 6$) to nonresponders ($n = 3$) in baseline (**E**) and on-treatment biopsies from patients with melanoma receiving combination nivolumab/pembrolizumab and ipilimumab (**F**). Benjamini–Hochberg P_{adj} values shown. **G,** Kaplan–Meier curves showing overall survival of 72 patients with melanoma treated with anti-PD-1 or anti-PD-1 and anti-CTLA-4 therapy stratified by high and low expression of indicated chemokines. Survival curves were compared with the log-rank test. **H,** Correlation of expression of indicated chemokine and numbers of intratumoral $CD8^+$ T cells in 56 biopsies of metastatic melanoma taken prior to checkpoint blockade, with each case annotated by response to therapy. Correlation tested with Pearson product moment correlation coefficient.

Published OnlineFirst October 21, 2019; DOI: 10.1158/1078-0432.CCR-19-1868

anti-PD-1/anti-CTLA-4 (Supplementary Fig. S1B). Analysis of tumor supernatants confirmed that several chemokines including CCL5, CCL22, CCL17, CXCL9, and CXCL10 were significantly upregulated at the protein level following dual blockade of PD-1 and CTLA-4 (**Fig. 1D**), whereas blockade of either PD-1 or CTLA-4 alone resulted in modest increases in chemokine production (Supplementary Fig. S1C).

We next analyzed the relevance of these chemokines in the context of patients with melanoma treated with either anti-PD-1 alone (nivolumab or pembrolizumab) or dual anti-PD-1/anti-CTLA-4 (ipilimumab) therapy as described previously (23). Strikingly, the expression of CXCL9, CXCL10, and CXCL11 was significantly higher in tumors isolated from responders at baseline (**Fig. 1E**) and on therapy (**Fig. 1F**). Furthermore, high expression of CXCL9 and CXCL10, in particular, was associated with improved patient survival and increased numbers of intratumoral $CD8^+$ T cells in these patients treated with immune checkpoint blockade (**Fig. 1G** and **H**). Analysis of a separate cohort of patients with melanoma treated exclusively with nivolumab single-agent therapy revealed that CXCL9, CXCL10, and CCL5 were also among the most highly upregulated genes in this cohort (Supplementary Fig. S2A; ref. 27). Moreover, analysis of gene expression data from the IMvigor 210 trial indicated that the expression of CXCL9 ($P = 0.0023$), CXCL10 ($P = 0.0074$), and CXCL11 ($P = 0.029$) were significant prognostic indicators in patients with metastatic urothelial carcinoma treated with atezolizumab, were expressed to a greater extent in responders than nonresponders, and correlated with the extent of T-cell infiltrate (Supplementary Fig. S2B–S2D). In contrast, the expression of other chemokines CCL5, CCL2, CCL17, and CCL22 did not correlate with survival (Supplementary Fig. S2B), despite also correlating with immune cell infiltrate (Supplementary Fig. S2D). In contrast, using data from both the METABRIC triple-negative breast cancer (Supplementary Fig. S3A; $n = 279$) and the TCGA melanoma cohorts (Supplementary Fig. S3B; $n = 369$), we identified that, in patients treated with standard-of-care therapies, CXCL9, CXCL10, CXCL11, CCL2, CCL17, CCL22, and CCL5 expression were all significantly associated with improved patient survival (Supplementary Fig. S3A and S3B) and was associated with a significant increase in the CTC gene score within patient's tumors, suggesting that the increased survival of patients with high levels of these chemokines was likely an immune-dependent phenomenon (Supplementary Fig. S3C). Taken together, these data indicate that responses to immune checkpoint blockade are associated with the expression of the CXCR3 ligands CXCL9 and CXCL10, particularly patients treated with the combination of anti-PD-1 and anti-CTLA-4. This led us to investigate the requirement for these chemokines in the therapeutic effect evoked by immune checkpoint blockade.

CXCR3 neutralization abrogates the efficacy of immune checkpoint blockade and prevents the infiltration of $CD8^+$ T cells following therapy

To investigate the role of CXCL9 and CXCL10 in the therapeutic effect mediated by dual PD-1/CTLA-4 blockade, we first utilized a blocking mAb for the CXCR3 receptor (**Fig. 2A**). Strikingly, the blockade of CXCR3 significantly reduced the efficacy of anti-PD-1/anti-CTLA-4 treatment leading to enhanced tumor growth (**Fig. 2B**), reduced survival of mice (**Fig. 2C**), and increased size and weight of tumors when tumors were excised at day 7 post-treatment (**Fig. 2D** and **E**). To determine whether this effect was broadly applicable to other cancer models, we also investigated this in the context of mice bearing MC38, E0771, or B16F10-ova tumors. In all cases, the antitumor effect mediated by dual agent anti-PD-1 and anti-CTLA-4 therapy was reduced by coadministration of an anti-CXCR3 antibody (**Fig. 2F–H**). Given that CXCR3 ligands are also important in the context of patients treated with atezolizumab as a single agent (Supplementary Fig. S2), we further assessed the importance of CXCR3 in a model that was sensitive to PD-1 inhibition alone. To this end, we treated less established AT-3ova tumors (day 7 postinoculation) using anti-PD-1 alone, which also resulted in significant therapeutic effects that were CXCR3 dependent (Supplementary Fig. S2E). Taken together, these data demonstrate the critical importance for the CXCR3/CXCR3 ligand axis for the therapeutic efficacy of anti-PD1/CTLA-4 therapy and next sought to investigate the underlying mechanism.

We have previously shown that dual PD-1/CTLA-4 blockade significantly enhances both $CD8^+$ and $CD4^+$ T-cell effector functions in this model and that the therapeutic efficacy of this combination therapy is dependent on both $CD8^+$ and $CD4^+foxp3^-$ cells (19). We therefore investigated the effect of CXCR3 blockade on the number and activation phenotype of these subsets in the context of dual PD-1/CTLA-4 blockade. In agreement with previous observations, including our own (19, 38–40), dual PD-1/CTLA-4 blockade led to a significant increase in the proportion and number of $CD8^+$ T cells (**Fig. 3A**; Supplementary Fig. S4A). Dual blockade therapy also significantly increased the frequency of $CD3^+CD4^+foxp3^-$ T cells (**Fig. 3B**) while the numbers of other lymphocyte populations including NK cells (**Fig. 3C**) and $CD4^+foxp3^+$ T cells were unaffected (**Fig. 3D**). Strikingly, blockade of CXCR3 significantly reduced the number of $CD8^+$ T cells and $CD4^+foxp3^-$ cells following dual PD-1/CTLA-4 blockade, as determined by both flow cytometry and immunofluorescence analysis (**Fig. 3A, B,** and **E**). In contrast, the frequency of other immune cell populations, including $CD4^+foxp3^+$ and $NK1.1^+$ NK cells, were not significantly reduced by CXCR3 blockade (**Fig. 3C** and **D**). Given that the expression of CXCR3 ligands has previously been linked to T-cell priming (41) as well as playing a role in trafficking (13), we investigated whether blockade of these receptors may also potentially impact the function of T cells within the tumor microenvironment in addition to their recruitment to the tumor. As expected, we observed that the combination of PD-1 and CTLA-4 significantly enhanced the production of both IFNγ and TNFα intratumorally in both the $CD8^+$ and $CD4^+foxp3^-$ subsets (**Fig. 3F**), consistent with our previous observations (19). Notably CXCR3 blockade significantly reduced the production of IFNγ and TNFα of $CD8^+$ and $CD4^+foxp3^-$ T cells, but not NK cells, in the setting of dual PD-1/CTLA-4 blockade (**Fig. 3F**; Supplementary Fig. S4B), suggesting that intratumoral expression of CXCR3 ligands enhanced their activation. However, CXCR3 blockade did not affect the expression of other markers associated with T-cell activation on either $CD8^+$ or $CD4^+foxp3^-$ cells including Ki67 (proliferation), PD-1/TIM-3, or tbet (**Fig. 3G**; Supplementary Fig. S4C). We next sought to identify whether the importance of CXCR3 for the therapeutic effects of dual PD-1/CTLA-4 blockade stemmed from enhanced CXCR3-dependent recruitment of T cells to the tumor site and/or local effects of CXCL9/10 on T-cell function. To address this, we repeated our therapeutic studies in the context of S1PR1 blockade, using FTY720. Treatment of mice with FTY720 significantly reduced the therapeutic efficacy of dual PD-1 and CTLA-4 blockade, to a similar extent as anti-CXCR3 (**Fig. 3H**). Moreover, blockade of CXCR3 did not affect the capacity of OT-I T cells to produce cytokines when cocultured with tumor cells *in vitro* (Supplementary Fig. S4D). Taken together, these data suggest that CXCR3-mediated enhancement of T-cell cytokine production *in vivo* is associated with enhanced migration of

Published OnlineFirst October 21, 2019; DOI: 10.1158/1078-0432.CCR-19-1868

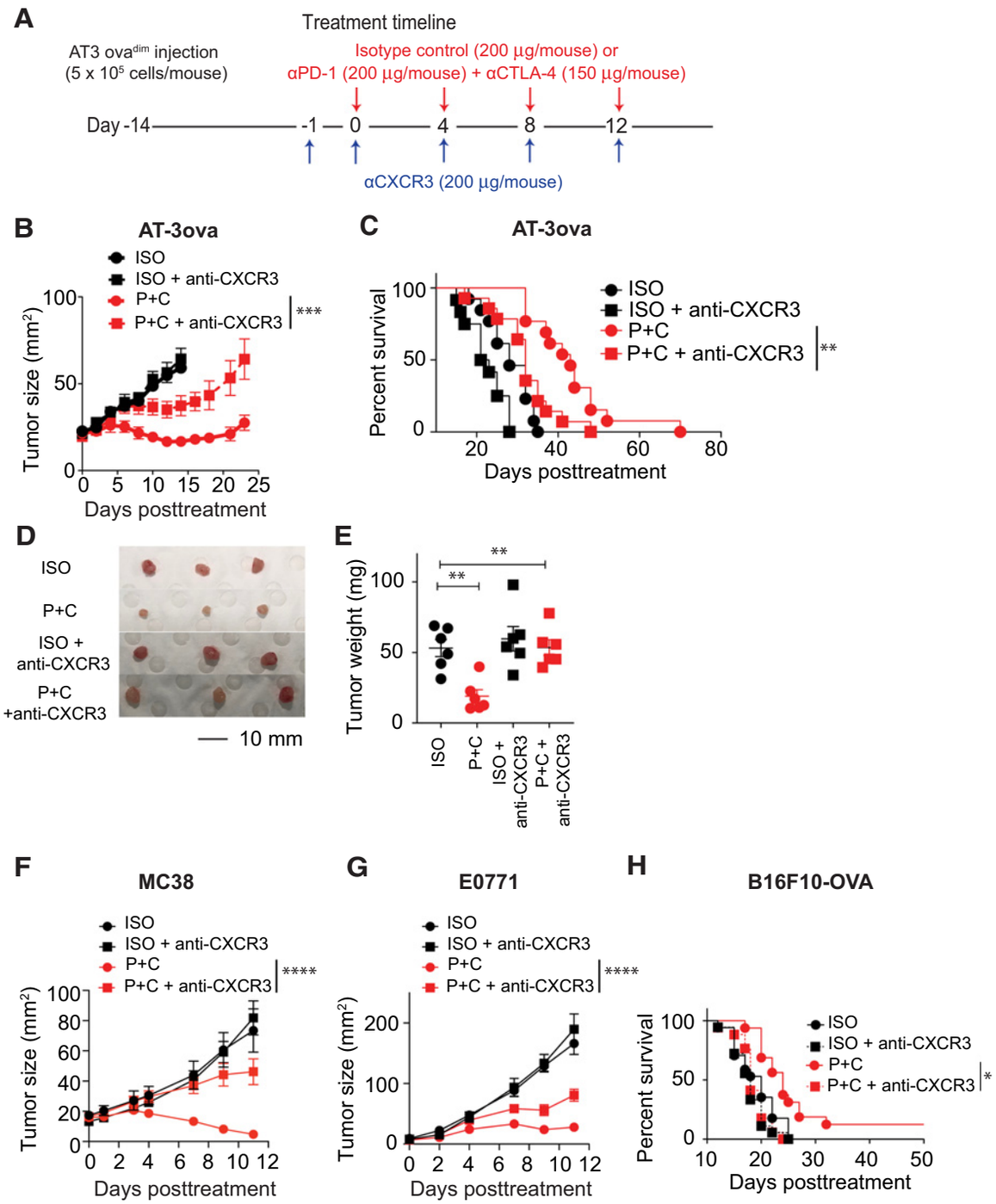

Figure 2.

CXCR3 blockade abrogates therapeutic efficacy of dual PD-1 and CTLA-4 blockade. **A,** C57BL/6 mice were injected subcutaneously with 5×10^5 AT-3ova cells and allowed to establish for 14 days before dual treatment with anti-PD-1 (200 µg/mouse) and anti-CTLA-4 (150 µg/mouse) ± anti-CXCR3 (200 µg/mouse). CXCR3 blockade was given on days 13, 14, 18, 22, and 26. Tumor growth (**B**) and survival (**C**) was assessed. Data shown as the mean ± of 6–8 mice/group of a representative experiment of $n = 3$. Survival is shown as combined data of two independent experiments. **, $P < 0.005$; *, $P < 0.05$ (determined by two-way ANOVA and Mantel–Cox test). Data points for ISO and P+C treated are included in **Fig. 1B**. **D** and **E,** Representative sizes (**D**) and weights (**E**) of tumors harvested 7 days posttreatment. A representative experiment of $n > 3$ is shown. **F–H,** C57BL/6 mice were injected with 3×10^5 MC38 cells (s.c.) and allowed to establish for 12 days ($n = 6$ mice per group). A total of 1.5×10^5 E0771 cells (intra mammary fat pad) and allowed to establish for 3 days ($n = 5$–8 per group of representative experiment $n = 2$; **G**) or 2×10^5 B16F10-OVA^{dim} cells were injected (s.c.; **H**) and allowed to establish for 4 days ($n = 16$–17 mice per group) before dual treatment with anti-PD-1/anti-CTLA-4 ± anti-CXCR3, as per **B**, except for MC38, which received only two doses of combined therapy.

Published OnlineFirst October 21, 2019; DOI: 10.1158/1078-0432.CCR-19-1868

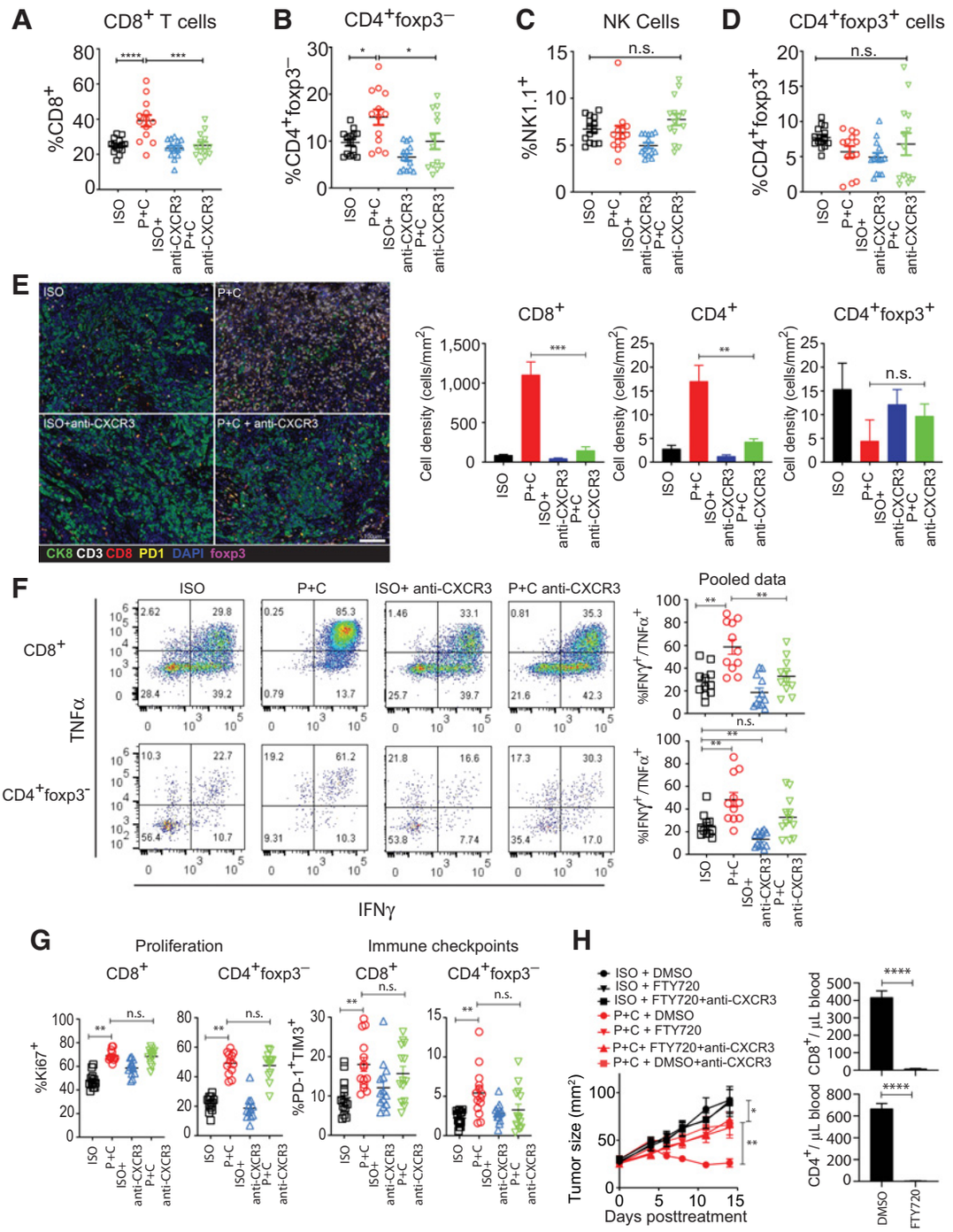

Figure 3.

CXCR3 blockade inhibits dual PD-1 and CTLA-4 blockade-induced $CD8^+$ T-cell migration and activation. C57BL/6 mice were injected subcutaneously with 5×10^5 AT-3ova cells and allowed to establish for 14 days before dual treatment with anti-PD-1 and anti-CTLA-4 ± anti-CXCR3 as per **Fig. 2**. On day 21 (7 days posttreatment) TIL infiltrate was analyzed as a percentage of $CD45^+$ cells; $CD8^+$ T cells (**A**), $CD4^+foxp3^-$ (**B**), $NK1.1^+$ cells (**C**), and $CD4^+foxp3^+$ cells (**D**). **E,** T-cell infiltrate quantified by immunofluorescence staining. Shown are representative images and quantification of three tumors per group. **F,** IFNγ and TNFα expression in $CD8^+$ and $CD4^+foxp3^-$ T cells was assessed. Shown are concatenated data from 6 mice (left) and quantification from two independent experiments (right). **G,** Ki67, PD-1, and TIM3 expression was determined in $CD8^+$ and $CD4^+foxp3^-$ T cells. **A–D**, **F**, and **G,** Data represent combined data of two independent experiments with $n = 11$–15 per group. **H,** Where indicated, mice were dosed with either the S1PR1 inhibitor FTY720 (25 mg/kg) or DMSO control on days 13 and 14 post tumor inoculation, and every 2 days subsequently. Right, numbers of $CD8^+$ and $CD4^+$ T cells collected from blood three days post initial FTY720 administration. Data are represented as the mean ± SEM of 6–7 mice per group (****, $P < 0.0001$; ***, $P < 0.001$; **, $P < 0.01$ one-way; n.s., not significant, one-way ANOVA or two-way ANOVA).

Published OnlineFirst October 21, 2019; DOI: 10.1158/1078-0432.CCR-19-1868

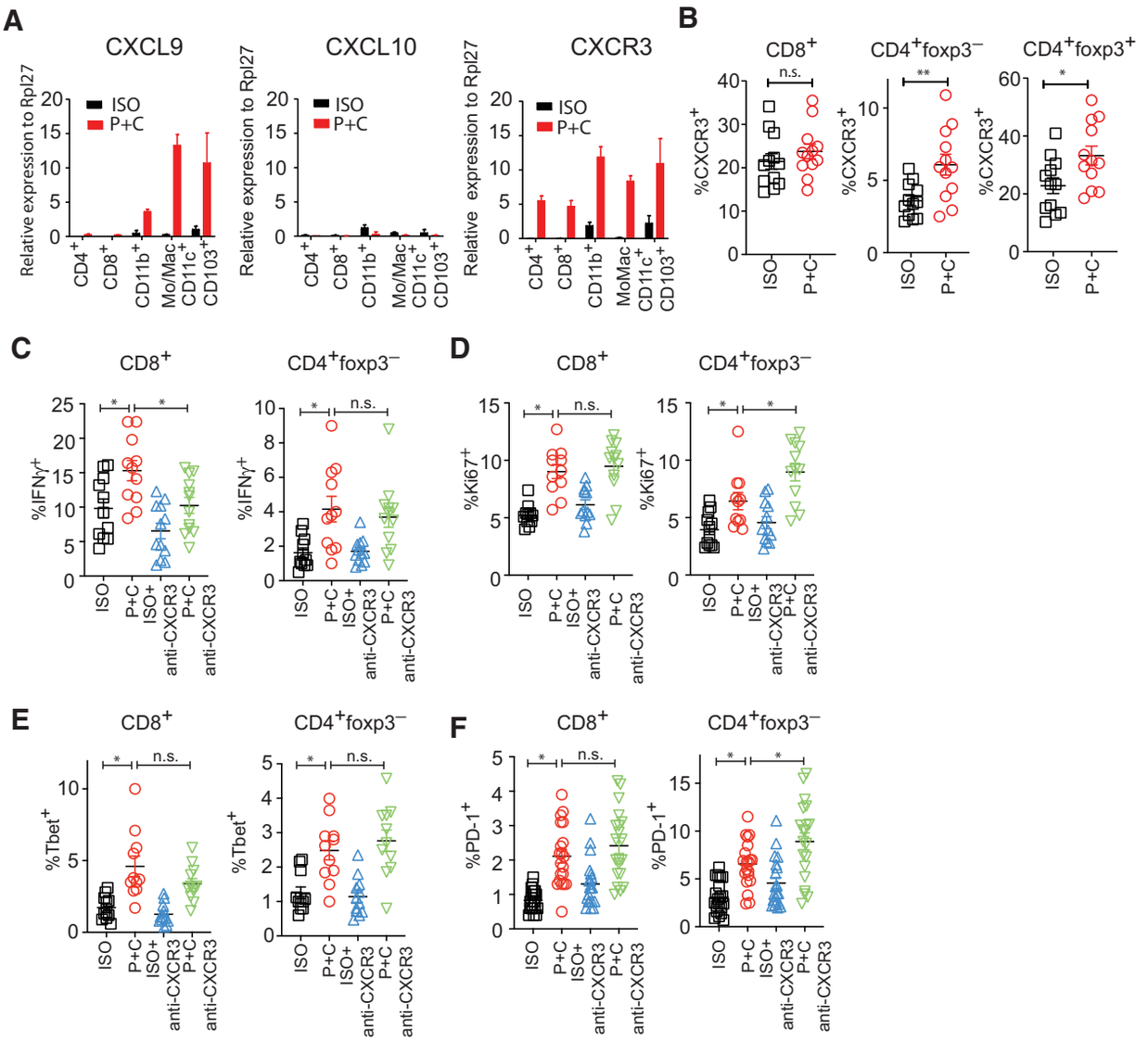

Figure 4.

CXCR3 and its ligands modulate T-cell priming within the tumor DLNs. DLNs were harvested from AT-3ova tumor bearing C57BL/6 mice following treatment with dual anti-PD-1 and anti-CTLA-4 ± anti-CXCR3 as per **Fig. 2**. **A,** Indicated immune cell populations were isolated using FACS and CXCL9, CXCL10, and CXCR3 expression was assessed by qRT-PCR. Expression is shown relative to the Rpl27 housekeeping gene and is representative of triplicate qRT-PCR reactions pooled from $n = 4$ mice per group. **B–F,** $CD8^+$ and $CD4^+foxp3^-$ T cells were assessed by flow cytometry for expression of CXCR3 (**B**), IFNγ (**C**), Ki67 (**D**), Tbet (**E**), and PD-1 [**F**;*, $P < 0.01$; **, $P < 0.01$; n.s., not significant, one-way ANOVA (**C–F**) or unpaired *t* test (**B**)]. Data are representative of $n = 12$ per group from two pooled experiments.

T cells to the tumor site which creates a more favorable environment for T-cell activation.

CXCR3 blockade affects the priming of $CD8^+$ T cells within the tumor draining lymph node

Given that we have previously shown that the therapeutic effects of anti-PD-1/anti-CTLA-4 are dependent on both $CD4^+foxp3^-$ and $CD8^+$ T cells and are associated with activation of these cells in the tumor draining lymph nodes (DLN; ref. 19), we further investigated the phenotype of these cells in the DLNs in the context of CXCR3 blockade. To investigate a potential role for CXCL9/CXCL10: CXCR3 interactions we first evaluated the expression of these genes in cells isolated from DLNs of tumor-bearing mice following PD-1/CTLA-4 blockade. This analysis revealed that CXCL9 and CXCR3 were significantly upregulated within tumor DLNs (**Fig. 4A** and **B**). We therefore investigated the effect of CXCR3 blockade on T-cell activation within tumor DLNs. In line with our previous observations, dual blockade of PD-1 and CTLA-4 led to the activation of both $CD8^+$ and $CD4^+foxp3^-$ T cells within DLNs in terms of IFNγ production, proliferation, and expression of tbet and PD-1 (**Fig. 4C–F**). Strikingly, and similar to our observations within the tumor microenvironment, blockade of CXCR3 significantly reduced the production of IFNγ by $CD8^+$ T cells isolated from tumor DLNs (**Fig. 4C**), while other parameters such as the expression of Ki67, tbet, and PD-1 were

Published OnlineFirst October 21, 2019; DOI: 10.1158/1078-0432.CCR-19-1868

unaffected (**Fig. 4D–F**). Interestingly, while CXCR3 blockade did not modulate the expression of IFNγ (**Fig. 4C**) or tbet (**Fig. 4E**) by $CD4^+foxp3^-$ cells in the DLNs, it did increase their expression of Ki67 (**Fig. 4D**) and PD-1 (**Fig. 4F**). Taken together, these data indicate that dual PD-1/CTLA-4 blockade not only induces CXCR3-dependent migration of $CD8^+$ T cells into the tumor site, but also that CXCR3 ligands modulate the activation of both $CD8^+$ and $CD4^+foxp3^-$ cells both at the tumor site and within DLNs.

Intratumoral CXCL9 is predominantly secreted from macrophages following immune checkpoint blockade

We next assessed the mechanism and cell types that were responsible for the generation of CXCR3 ligands following immune checkpoint blockade. One possibility was that the production of CXCL9 and CXCL10 was mediated by tumor cells, because AT-3ova cells produced CXCL9 and CXCL10 following stimulation with IFNγ and TNFα *in vitro* (Supplementary Fig. S5A and S5B). To assess the importance of tumor-derived CXCL9/CXCL10 for the therapeutic effect of dual PD-1/CTLA-4 blockade, we generated AT-3ova cells that did not express CXCL9 or CXCL10 using CRISPR-Cas9–mediated deletion of these genes. The resulting cells produced negligible amounts of CXCL9/10 *in vitro* following dual TNFα and IFNγ stimulation (Supplementary Fig. S5C). However, loss of CXCL9 and CXCL10 production by AT-3ova tumor cells did not significantly affect their responsiveness to dual PD-1/CTLA-4 blockade (**Fig. 5A**) nor the level of CXCL9 within the tumor microenvironment following therapy (**Fig. 5B**). These data suggested that host cells were the major source of CXCL9 in the context of combination therapy that was critical for the therapeutic effect. Accordingly, we assessed the cell types responsible for the production of CXCL9 and CXCL10 in tumors of mice undergoing immune checkpoint therapy. Following dual PD-1/CTLA-4 blockade, on a per cell basis, CXCL9 was predominantly expressed in a monocyte/macrophage (Mo/Mac) population, defined as $CD11b^+Ly6C^{int}CD11c^+F4/80^+$ (**Fig. 5C** and **D**; Supplementary Fig. S6A). Moreover, dual anti-PD-1/anti-CTLA-4 treatment evoked a strong infiltration and/or differentiation of macrophages as shown by an increased proportion of these cells (Supplementary Fig. S6B and S6C) and a significant upregulation of a macrophage gene signature in treated tumors (**Fig. 5E**). Moreover, these cells expressed high levels of CD64 and MHCII, phenotypic markers associated with monocytes/macrophages, thus confirming their identity as macrophages (Supplementary Fig. S6D). Therefore, although CXCL9 production was increased in $CD103^+$ cDC1s ($CD11c^+CD103^+CD11b^-$) and tumor/stromal cells ($CD45^-$) following dual PD-1/CTLA-4 blockade (**Fig. 5C** and **D**), given their increased frequency relative to $CD103^+$ DCs (Supplementary Fig. S6C and S6E), Mo/Macs were the predominant source of CXCL9. Indeed, Mo/Macs accounted for 38.1% of CXCL9-positive cells following dual PD-1/CTLA-4 blockade with conventional $CD11b^+CD11c^+MHCII^+$ DCs (27.5%) and $CD45.2^-$ cells (stroma/tumor; 14.7%) making up the other major $CXCL9^+$ populations (**Fig. 5F**; Supplementary Fig. S6F). These experiments also revealed that B cells were not a major source of CXCL9 (Supplementary Fig. S6G). Macrophages were also a major source of CXCL9 in MC38 tumors (**Fig. 5G**) and analysis of an independent, previously generated single-cell RNA-seq dataset of tumor-infiltrating immune cells in the CT26 tumor model (35) revealed that CXCL9 and CXCL10 were predominantly expressed by immune cells that also coexpressed the macrophage markers F4/80 and CD64 (**Fig. 5H**), confirming this observation was applicable to multiple tumor models. To analyze CXCL10 in the context of dual PD-1/CTLA-4 blockade in the absence of an antibody suitable for flow cytometry, we also FACS sorted the relevant immune populations and analyzed CXCL9/10 at the transcriptional level. This analysis confirmed that Mo/Mac cells produced significantly more CXCL9 in the context of dual checkpoint blockade and that these cells also produced large amounts of CXCL10 mRNA following therapy (Supplementary Fig. S6A).

Production of CXCL9 and CXCL10 is IFNγ dependent

Given the known key role of IFNγ and TNFα in modulating CXCL9/10 expression in alternative contexts (13, 42), we next assessed their importance in driving chemokine expression *in vivo* in the context of immune checkpoint blockade. We found that IFNγ and TNFα levels were significantly enhanced in the context of dual checkpoint blockade (in comparison to single agent PD-1 or CTLA-4 blockade) and that both CXCL9 and CXCL10 expression was highly correlated with IFNγ and TNFα production (**Fig. 6A**). We next sought to confirm these observations in the IMvigor210 trial cohort where CXCL9 and CXCL10 expression was associated with improved responses to atezolizumab (anti-PD-L1; Supplementary Fig. S2B). Both CXCL9- and CXCL10-high tumors were significantly enriched for both IFNγ and TNFα gene signatures (**Fig. 6B**). To formally test the requirement of IFNγ and TNFα for CXCL9 production following dual checkpoint blockade, we analyzed the production of CXCL9 by Mo/Macs and $CD11b^+CD103^+$DCs in the context of either IFNγ or TNFα neutralization. These results revealed that IFNγ was critical for CXCL9 production while no significant difference was observed following TNFα neutralization (**Fig. 6C**). To confirm this directly, we stimulated tumor-infiltrating leukocytes *ex vivo* with IFNγ and/or TNFα which revealed that macrophages, DCs, and $CD45^-$ cells upregulated CXCL9 *ex vivo* in response to IFNγ stimulation alone (**Fig. 6D**). Consistent with our previous data, macrophages isolated from tumors in mice treated with anti-PD-1 and anti-CTLA-4 secreted high amounts of CXCL9 that could not be further enhanced by IFNγ, suggesting that this IFNγ pathway was already activated *in vivo*. Notably, these effects were also observed in $BATF3^{-/-}$ mice, confirming that these effects were independent of $CD103^+$ DCs (**Fig. 6E**). However, we did observe that the overall levels of CXCL9 production by macrophages were lower in $BATF3^{-/-}$ mice, suggesting that $CD103^+$ DCs indirectly contributed to the production of CXCL9 by these cells. Taken together, these data demonstrated that Mo/Mac cells are the major source of tumor-derived CXCL9 and CXCL10 after dual PD-1/CTLA-4 blockade and that this expression is driven by IFNγ that is induced following combination therapy.

Macrophages are essential for dual PD-1/CTLA4 therapeutic efficacy

To investigate the requirement for macrophages for CXCL9/10 production following dual PD-1/CTLA-4 blockade, we depleted these cells using an anti-F4/80 antibody (Supplementary Fig. S6H), which resulted in a complete abrogation of the therapeutic efficacy of dual PD-1/CTLA-4 blockade (**Fig. 7A**). Depletion of macrophages also attenuated the increased production of CXCL9 (**Fig. 7B**) and infiltration of $CD8^+$ and $CD4^+foxp3^-$ cells within tumors following dual PD-1/CTLA-4 blockade (**Fig. 7C**). Similarly, IFNγ neutralization also attenuated increased infiltration of $CD8^+$ and $CD4^+foxp3^-$ cells, highlighting the link between IFNγ, macrophages, and CXCL9 production. To investigate the clinical significance of macrophage-derived CXCR3 ligands (CXCL9/CXCL10/CXCL11), we next sought to determine the source of these chemokines in human tumors and their prognostic significance.

Analysis of single-cell RNA-seq datasets in melanoma (29), lung carcinoma (32), and head and neck cancer cohorts (31) revealed that

Published OnlineFirst October 21, 2019; DOI: 10.1158/1078-0432.CCR-19-1868

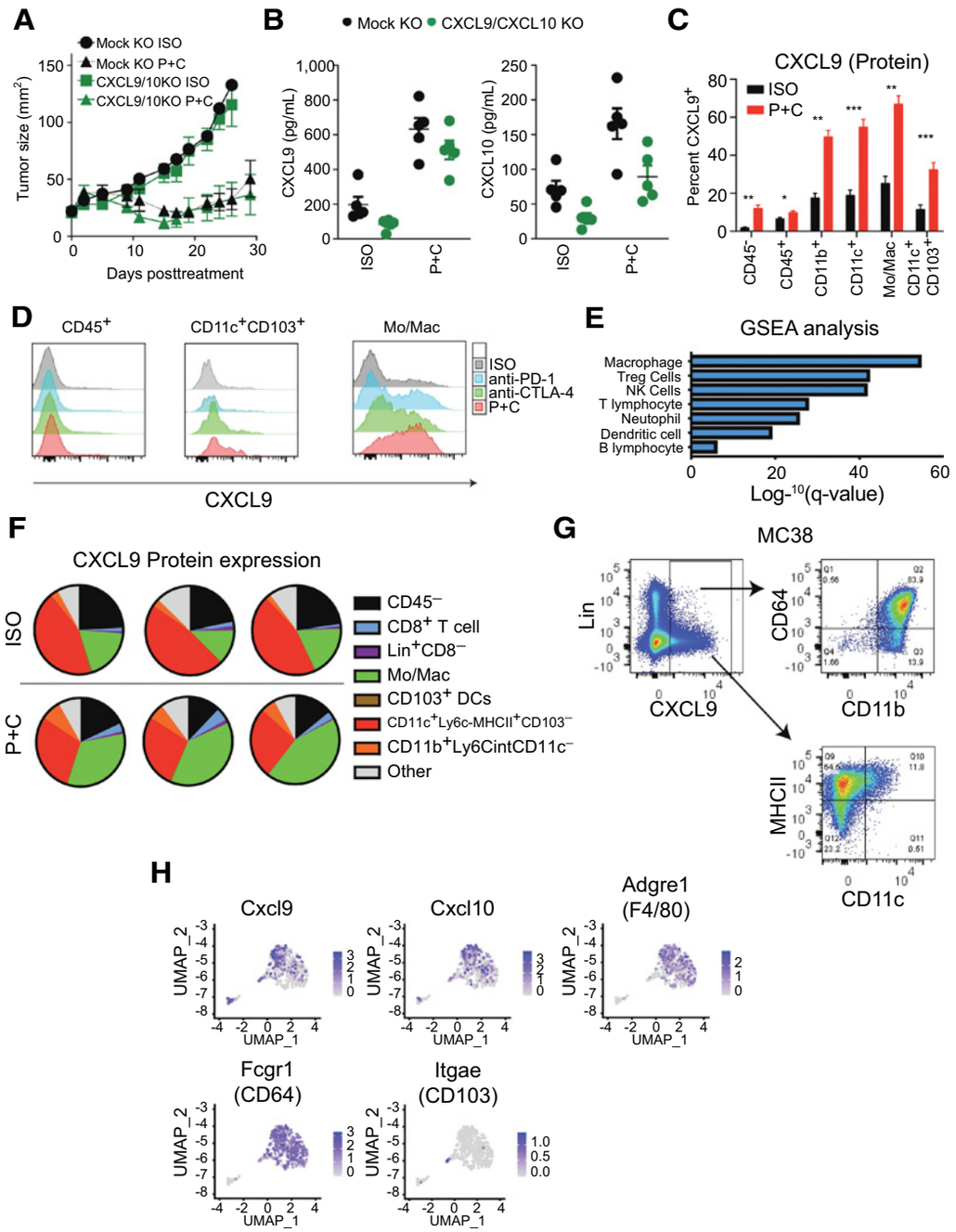

Figure 5.

Macrophages are the major source of intratumoral CXCL9 and CXCL10 following dual combination therapy. C57BL/6 mice were injected subcutaneously with either 5 $\times$ 10^5 control AT-3ova (Mock KO) or CXCL9/CXCL10 double KO AT-3ova cells and allowed to establish for 14 days (**A**). Mice were then treated with either dual anti-PD-1 (200 μg/mouse) and anti-CTLA-4 (150 μg/mouse) or isotype control (200 μg/mouse). Treatment was repeated on days 18, 22, and 26. On day 21, tumors were collected from mice and CXCL9 and CXCL10 production assessed by chemokine bead array as per **Fig. 1A** and **B**. Data shown are the mean ± SEM of 5–6 mice per group, of a representative experiment ($n = 2$). *, $P < 0.05$, n.s., not significant assessed by one-way ANOVA. **C**, **D,** and **F,** Intracellular CXCL9 staining was performed *ex vivo* in the presence of golgi plug/golgi stop for 3 hours at 37°C. $n = 3$ mice per group, two representative experiments. **C,** CXCL9 production per cell type before and after therapy. **D,** CXCL9 staining in indicated populations shown as representative histograms. **E,** Tissue enrichment scores for the top 200 genes upregulated in tumors treated with anti-PD-1 and anti-CTLA-4 relative to isotype control treated mice. **F,** Pie charts indicating the source of CXCL9 by cell type. Each pie represents one mouse from a representative experiment. **G,** C57BL/76 mice were injected with MC38 subcutaneously and 19 days postinoculation expression of CXCL9 by tumor-infiltrating myeloid cells was determined. **H,** Expression of Cxcl9, Cxcl10, Adgrel (F4/80), Fcgr1 (CD64), and Itgae (CD103) in CT26 tumor-infiltrating immune cells as determined by single-cell RNA-seq (35). UMAP embedding of single cells in macrophage cluster (larger population) and fibroblast cluster (smaller population bottom left) identified as per the original study are shown, with color intensity representing normalized gene expression level.

Published OnlineFirst October 21, 2019; DOI: 10.1158/1078-0432.CCR-19-1868

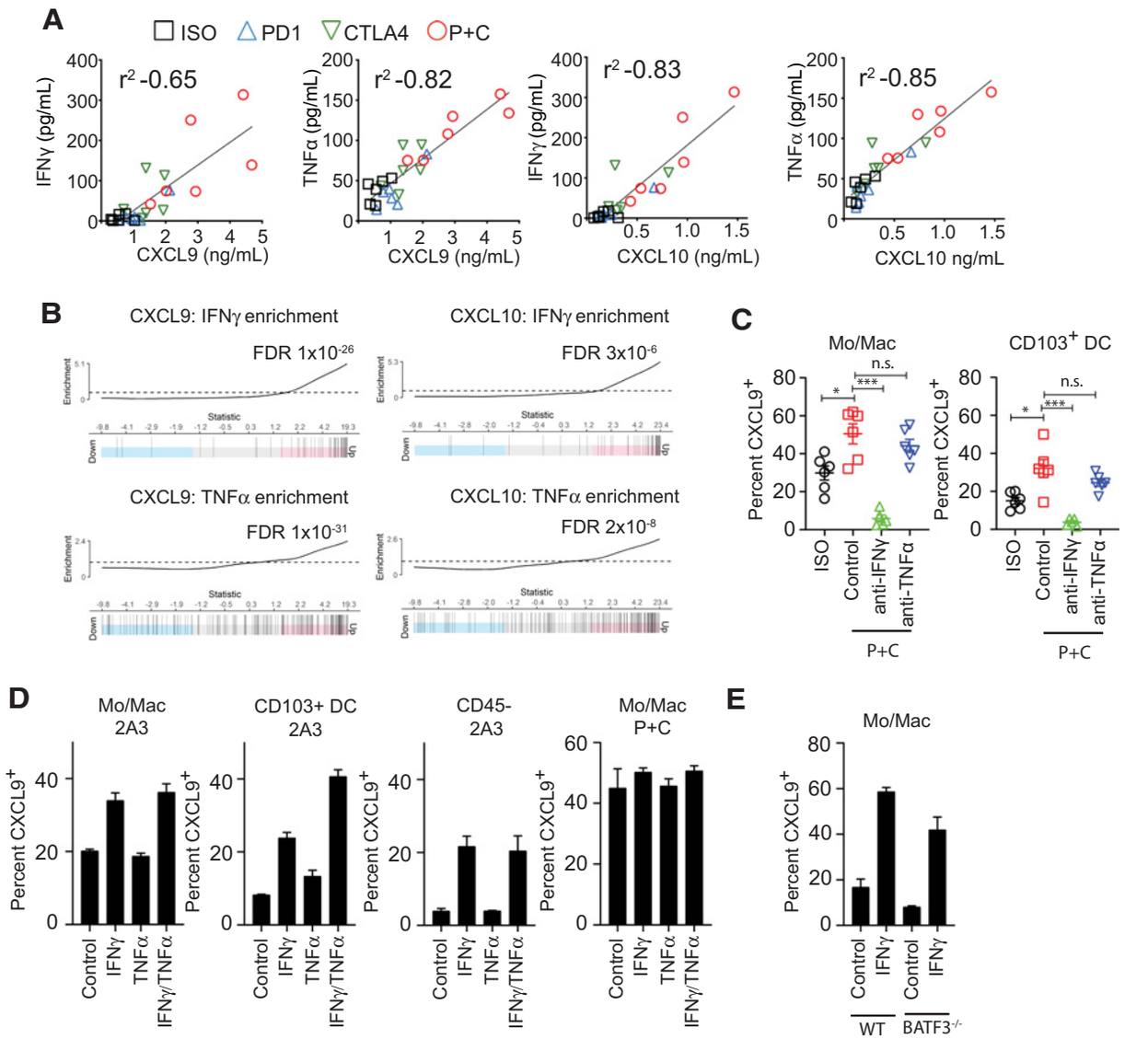

Figure 6.

IFNγ is sufficient to induce CXCL9 expression from intratumoral macrophages. **A,** Correlation of IFNγ or TNFα and CXCL9/CXCL10 production as determined by cytometric bead array of tumor samples obtained as per **Fig. 1**. Data is represented as $n = 6$ mice per group from two independent experiments. R^2 values determined by linear regression analysis. **B,** IFNγ and TNFα gene signature enrichment scores for CXCL9- and CXCL10-high tumors in patients with urothelial cancer treated with atezolizumab (IMvigor210 trial). **C,** AT-3ova tumor-bearing mice were treated as per **Fig. 5A** with the additional treatment of anti-IFNγ or anti-TNFα (250 μg/mouse) on days 14 and 18. Expression of CXCL9 in MoMacs and CD103$^+$ dendritic cells determined in $n = 6$ mice per group. **D** and **E,** AT-3ova tumor-bearing C57BL/6 wild-type or BATF3$^{-/-}$ mice were treated as per **Fig. 5A**. Seven days posttreatment, tumor-infiltrating lymphocytes were dissociated and stimulated for 3 hours with 1 ng/mL IFNγ and/or TNFα in the presence of Golgi Plug/Stop. Expression of CXCL9 in Mo/Macs or CD103$^+$ DCs was determined by flow cytometry (*, $P < 0.05$; **, $P < 0.01$; ***, $P < 0.001$, not significant, one-way ANOVA).

macrophages were the predominant cell type responsible for the production of CXCL9, CXCL10, and CXCL11 (**Fig. 7D** and **E**; Supplementary Fig. S7A and S7B). Of note, within the lung carcinomas studied by Zilonis and colleagues (32), multiple DC and macrophage (tMac1-9) subpopulations were defined but CXCL9-11 were more highly expressed by CD68-expressing macrophages than dendritic cells, including the CLEC9A$^+$ cDC1 population (**Fig. 7E**). This was consistent with all human datasets analyzed where CXCL9-11 production was also detected in other immune cell populations such as dendritic cells, but consistently to a lesser extent than macrophages (**Fig. 7D**; Supplementary Fig. S7A and S7B). Utilizing the melanoma dataset of Sade-Feldman and colleagues, derived from single-cell RNA-seq analysis before and after immune checkpoint blockade, we were able to investigate the expression of these chemokines in the context of immunotherapy (29). Differential gene expression analysis of macrophages in responders and nonresponders revealed that CXCR3 ligands, and in particular CXCL10 and CXCL11, were more abundantly expressed in macrophages from responding patients (**Fig. 7F** and **G**). Further analysis of the macrophage transcriptome identified a unique macrophage gene signature that included CXCL10

Published OnlineFirst October 21, 2019; DOI: 10.1158/1078-0432.CCR-19-1868

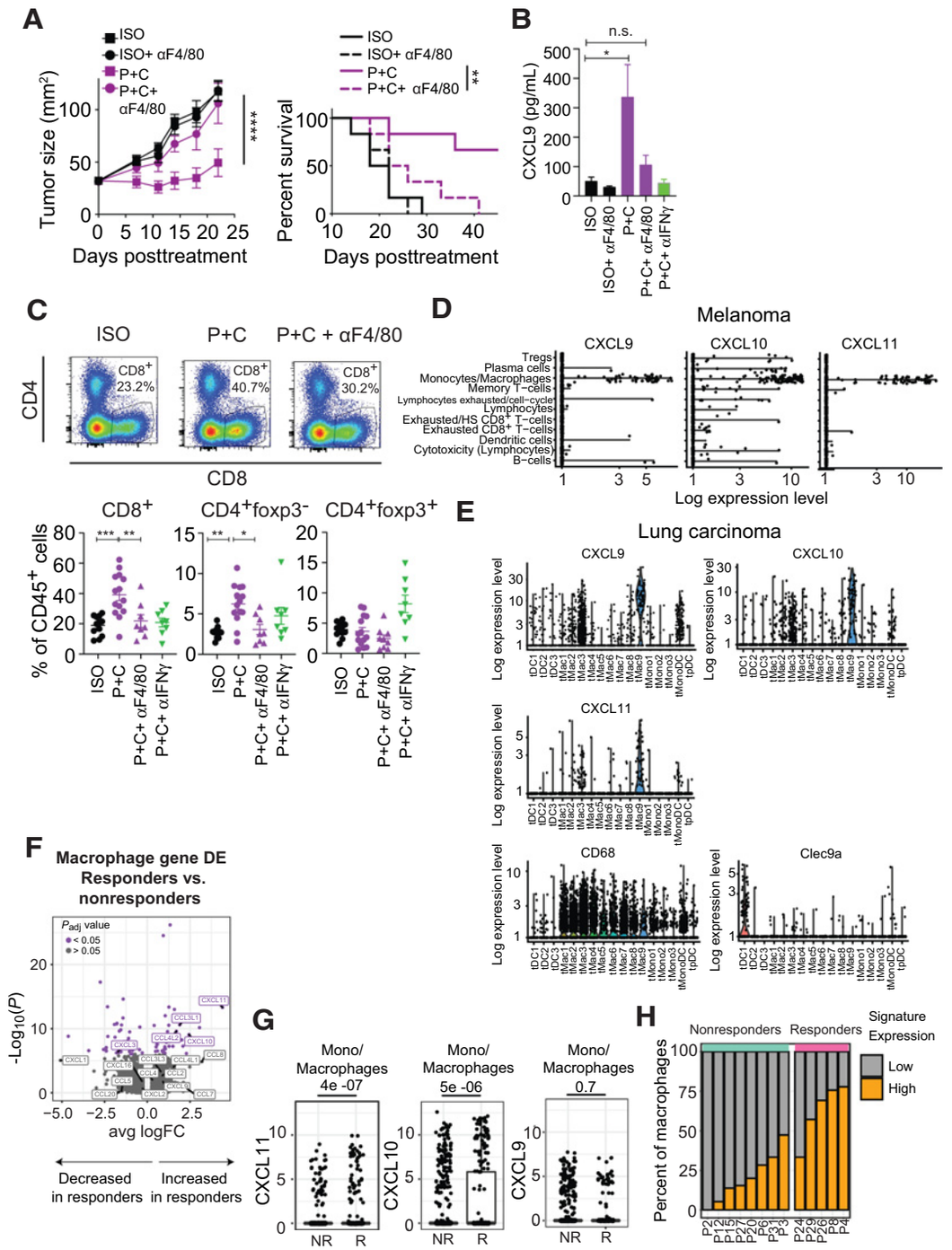

Figure 7.

Generation of CXCR3 ligands by macrophages is critical for the efficacy of immune checkpoint blockade. **A–C,** C57BL/6 mice were injected subcutaneously with 5×10^5 AT-3ova cells and allowed to establish for 14 days before dual treatment with anti-PD-1, anti-CTLA-4 and/or anti-F4/80 (100 μg/mouse) as per **Fig. 2**. **A,** Tumor size (left) and survival (right) of $n = 6$ mice per group from a representative experiment of $n = 2$. **B,** CXCL9 production by tumors *ex vivo* following therapy, $n = 3$–7 per group. **C,** FACS plots from concatenated samples (top) and individual data points ($n = 8$–14 per group; bottom) are shown. Expression of CXCL9, CXCL10, CXCL11, CD68, and CLEC9a by cell subset in all patients at baseline in a cohort of patients with metastatic melanoma (**D**) and a cohort of patients with lung cancer (**E**) that underwent single-cell RNASeq (melanoma; 5,928 cells from 19 patients, lung carcinoma; Violin plots are shown with single-cell expression values overlayed). **F,** Single-cell differential gene expression analysis in macrophages in baseline melanoma samples from responders versus nonresponders. **G,** Box plot of CXCL9, CXCL10, and CXCL11 expression level in individual macrophages from baseline melanoma cases in relation to immune checkpoint blockade response. Significance determined by unpaired *t* test. **H,** Proportion of macrophages displaying chemokine signature in responders and nonresponders.

Published OnlineFirst October 21, 2019; DOI: 10.1158/1078-0432.CCR-19-1868

and CXCL11 that was more abundant in macrophages derived from patients that responded to immune checkpoint blockade (**Fig. 7H**; Supplementary Fig. S7C). Taken together, the data obtained from these patient samples strongly supports our preclinical observation that macrophages are a major source of CXCR3 ligands and are associated with responses to immune checkpoint blockade.

Discussion

Understanding the processes which govern responsiveness to immune checkpoint therapy as well as the transition from non-T-cell–infiltrated to inflamed tumors are two major frontiers in the field of cancer immunotherapy. A number of factors can contribute to these parameters, including the local tumor microenvironment, stromal stiffness, the production of factors that promote an immune exclusion phenotype (24, 43, 44) and an ineffective or inappropriate production of chemokines that either promote the recruitment of immunosuppressive subtypes (45, 46) or a failure to mount effective recruitment of antitumor T cells. In this study, we investigated chemokine production within tumors following effective therapy with immune checkpoint inhibitors (anti-PD-1 and anti-CTLA-4). This analysis showed that CXCL9 production was significantly induced in an IFNγ-dependent manner following therapy both at the transcriptional and protein level and that the production of CXCR3 ligands was critical for therapeutic efficacy. The requirement for the CXCL9:CXCR3 axis for the therapeutic efficacy of these immunotherapeutic treatments is consistent with previous data indicating that CXCL9/CXCL10:CXCR3 interactions govern immune cell infiltration into tumors prior to therapy (47) and following chemotherapy (10, 48, 49), IL2 treatment (50, 51), adoptive cellular therapy (12, 52, 53), bispecific antibodies (54), and that $CXCR3^{-/-}$ mice fail to elicit effective antitumor immune responses postvaccination and anti-PD-1 (55). These studies have shown that CXCL9 and CXCL10 can modulate antitumor immune responses evoked following several therapeutic approaches. Although our murine studies did not address the role of CXCL11 (as C57BL/6 mice do not express CXCL11), the data obtained from patients with cancer suggests that this chemokine is worthy of further attention in future studies. Notably, our data indicate that CXCL11 expression correlates with improved responses to atezolizumab and was the most significantly upregulated gene in macrophages isolated from patients responding to immune checkpoint blockade. Therefore, further studies investigating the role of CXCL11 in human cancers, and, in particular, its function relative to CXCL9 and CXCL10 would be of high relevance. Although our study focuses on the role of CXCR3 ligands in the response to immune checkpoint blockade, it does not preclude a role for other important chemokines such as CCL5, the expression of which was shown to correlate with enhanced antitumor immune responses and improved patient survival, particularly in the context of high CXCL9 expression (56). However, while CCL5 can potentially enhance antitumor immunity through the recruitment of $CCR5^+$ T cells and NK cells, protumoral roles of CCL5 have also been reported (57, 58). Therefore, strategies to enhance CXCL9/10/11 production may be more favorable to those designed to enhance CCL5 expression.

Our data indicating the importance of CXCL9/10/11: CXCR3 interactions for the efficacy of immune checkpoint blockade *in vivo* was supported by transcriptome analysis of patients treated with either atezolizumab (anti-PD-L1) or nivolumab (anti-PD-1), or a combination of ipilimumab and a PD-1 blocking antibody. In all cases, CXCL9/10/11 production was highly correlated with improved patient survival and their production was associated with an IFNγ gene signature. Given that single-cell RNA-seq analysis revealed that CXCR3 is highly expressed on $CD8^+$ and $CD4^+$ tumor-infiltrating lymphocytes in triple-negative breast cancer (59), it is highly likely that local production of CXCL9/10 can modulate T-cell recruitment and activation in human cancers. Interestingly, a similar observation has been reported in a study of 45 patients with melanoma treated with ipilimumab where the increased expression of IFNγ-dependent genes including CXCL9-11 was observed in patients undergoing a clinical response (60). Our analysis supports that these chemokines are also increased following anti-PD-1 and that they are crucial for therapeutic activity and correlate with patient prognosis. Therefore, strategies to enhance the expression and/or activity of CXCL9/10 may be expected to enhance the therapeutic efficacy of immune checkpoint blockade. Indeed, the use of a Dipeptidylpeptidase 4 (DPP4, CD26) inhibitor to preserve CXCL10 bioactivity was shown to enhance the efficacy of adoptive cellular therapy and immune checkpoint blockade (61, 62). Similarly, the localized application of a COX-2 inhibitor was shown to enhance therapeutic responses to anti-PD-1, associated with an increase in expression of CXCL9 and CXCL10 (63) and epigenetic modulators (EZH2i and DNMT1i) were shown to enhance antitumor immune responses associated with increased expression of CXCL9 and CXCL10 (64). However, given the broad nonspecific nature of these inhibitors, it is clear that more specific therapeutics to modulate the CXCL9/CXCL10 chemokines would be of significant interest.

Having established that CXCR3 was crucial to the antitumor efficacy of dual PD-1/CTLA-4 blockade, we next investigated the underlying mechanisms. We observed that CXCR3 blockade reduced $CD8^+$ T-cell infiltrate into tumors following dual PD-1/CTLA-4 blockade while the numbers of other immune cell populations such as $CD4^+$ Tregs and NK cells were not affected. This was somewhat surprising given that these cells express CXCR3 and expression of CXCL10 was shown to promote NK-cell infiltration into the NK-sensitive RMA-S cell line (65). However, these data may either reflect a higher dependency of $CD8^+$ T cells on CXCR3 for their migration into the tumor site following immune checkpoint blockade than other immune cell subtypes and/or our use of a T-cell–sensitive model where NK cells are unlikely to play a major role in the control of tumor growth. This hypothesis is consistent with the fact that CXCR3 expression was increased following T-cell activation by dual PD-1/CTLA-4 blockade. We did not investigate the role of CXCL9 and CXCL10 in recruiting other immune cell types, including myeloid cells. Intriguingly, because monocytes themselves express CXCR3, it is possible that CXCL9/10 production by monocytes/macrophages leads to the recruitment of more monocytes in a positive feedback loop.

Previous studies have shown that CXCL9 and CXCL10 can be secreted by multiple cell types including monocytes, endothelial cells, fibroblasts, inflammatory macrophages dendritic cells (particularly the cDC1 subtype) and tumor cells themselves (9, 12, 13, 66–68). In the context of cancer, previous data have suggested that tumor cells (68), $CD103^+$ DCs (9, 12, 69), or $CD11b^+$ cells (67) are major sources of CXCL9/10 within the tumor microenvironment. Notably, while we did observe that dual PD-1/CTLA-4 blockade enhanced CXCL9/10 production by $CD103^+$ DCs and the bulk $CD11b^+$ population, our data indicate that macrophages are the predominant source of CXCL9 and CXCL10 in the context of immune checkpoint blockade both in mice and in patients. This was supported by single-cell RNA-seq in patient datasets and alternative murine tumor models suggesting this is a pathway conserved in multiple tumor types.

Our analysis of single-cell RNA-seq data indicated that macrophages secreted higher levels of CXCL9-11 than dendritic cells in multiple

Published OnlineFirst October 21, 2019; DOI: 10.1158/1078-0432.CCR-19-1868

cancer cell types. This was also observed in the context of immunotherapy where the presence of CXCL10- or CXCL11-positive macrophages was a marker for benefit from immunotherapy. Although CXCL9 was not prognostic within this patient cohort, we cannot exclude the possibility that the low CXCL9 counts arose through technical limitation rather than a reduced expression of CXCL9 relative to the other CXCR3 ligands CXCL10 and CXCL11. Our data suggest that the production of CXCL9 and CXCL10 by the tumor cells themselves are dispensable for the therapeutic effect of anti-PD-1 and anti-CTLA-4 and that knockout of these genes from tumor cells had minimal impact on the overall concentration of these chemokines, particularly CXCL9, in the context of dual combination therapy. However, we cannot exclude a role for tumor-derived CXCL9/CXCL10 in tumors with low immune infiltrate where their overall contribution to CXCL9/CXCL10 levels maybe more pronounced. Interestingly, our data also suggest a greater increase in CXCL10 mRNA, relative to CXCL9 mRNA, in $CD45^-$ cells following combination therapy. Although this population includes tumor cells and other host cells such as stroma, it would be interesting to confirm this at the protein level in future experiments, particularly because we observed a significant decrease in CXCL10 protein levels within the tumor microenvironment following CRISPR-Cas9–mediated deletion of CXCL10 from tumor cells.

Moreover, our data do not discount the importance of CXCL9/10 from other cell types including $CD103^+$ DCs, which has previously been reported in the context of adoptive cellular therapy and immune checkpoint blockade (12, 69). The production of CXCL9/10 by these cells can enhance T-cell priming by facilitating DC:T-cell interactions and result in enhanced antitumor immunity. However, our data indicate a clear role for CXCR3-dependent migration of T cells into tumors and that the predominant cellular source of CXCL9/10 is macrophages. We believe one explanation for this apparent discrepancy is that while macrophages are critical for CXCR3-dependent recruitment of T cells through their production of CXCL9/10 in the tumor, CXCL9/10 production by other myeloid subsets, including $CD103^+$ DCs, is likely to be important for T-cell priming both within the tumor and in the DLN. Therefore, while our studies do not preclude an important role for CXCL9/10 production by DCs in promoting T-cell activation, they clearly indicate that macrophages are responsible for a significant proportion of these chemokines. Notably, the requirement for immune cell trafficking into tumors following immune checkpoint blockade is consistent with the emergence of new antigen-specific immune cells at the tumor site following therapy (70).

Although it was recently described that anti-TIM-3 therapy enhances CXCL9/10 production by $CD103^+$ DCs through direct modulation of TIM-3 expressed on $CD103^+$ DCs (9), such a direct mechanism is unlikely to contribute to the efficacy of PD-1 and CTLA-4 blockade, as PD-1 and CTLA-4 are not expressed on either DCs or the tumoral macrophages in our study. Instead, our data suggest that T-cell–mediated increases in IFNγ and TNFα production are critical for this effect. Indeed, we observed that the production of CXCL9 was dependent on IFNγ and TNFα, which is consistent with the role of STAT1 and NFκB in enhancing the transcriptional activity of CXCL9 (71, 72) and with a previous report that indicated that anti-PD-1 enhanced CXCL10 production from intratumoral $CD11b^+$ cells within tumors in an IFNγ-dependent manner in the context of adoptive cellular therapy (67). Transcriptome analysis of patient's tumors post immune checkpoint blockade indicated a robust correlation between the expression of IFNγ-related genes and CXCL9/CXCL10, suggesting that this mechanism is also important in patients. Given that mutations in both the JAK–STAT (73–75) pathway and in TNF signaling (76) have previously been reported as resistance mechanisms for immune checkpoint inhibitors, our data suggests that a failure to secrete CXCL9/CXCL10 by these tumors may represent an additional mechanism of immune escape.

Interestingly, the role of the CXCR3 receptor in the response to dual PD-1/CTLA-4 blockade was not limited to $CD8^+$ T-cell trafficking to the tumor site because CXCR3 blockade also modulated T-cell functionality in the DLNs. CXCR3 mRNA expression was increased on both $CD4^+$ and $CD8^+$ subsets following dual PD-1/CTLA-4 blockade and, although we did not observe increased expression of CXCR3 protein on $CD8^+$ T cells following dual PD-1/CTLA-4 blockade, this is potentially explained by CXCR3 internalization that has previously been reported (77). Blockade of CXCR3 reduced the production of IFNγ by $CD8^+$ T cells in DLNs and affected $CD4^+foxp3^-$ T-cell differentiation as shown by enhanced expression of PD-1 and the proliferation marker Ki67. The mechanism underlying this is yet to be fully determined but a role for CXCR3 ligands in promoting DC:T-cell interactions within interfollicular regions of lymph nodes following vaccination has been described previously (41, 78). Thus, it is tempting to speculate that CXCL9/CXCL10:CXCR3 interactions may play a similar role in tumor DLNs by promoting the aggregation of tumor-specific T cells and antigen presenting DCs. Interestingly in these studies showing a role for CXCR3 ligands in lymph node priming, the production of CXCL10 was predominantly by the $CD11b^+$ lymph node resident DCs while CXCL9 was predominantly expressed by stromal cells. While we did not observe significant expression of CXCL10 by $CD11b^+$ cells in our analysis, we cannot exclude that the expression of CXCL10 was restricted to an alternative immune subset and/or expressed at a different timepoint than analyzed in our experiments. Nevertheless, our data suggest a role for CXCL9/CXCR3 interactions within DLNs in the context of immunotherapy and this could potentially play a role in the spatial organization and consequent activation of both $CD8^+$ and $CD4^+$ T cells within the DLNs, as has been reported in the context of vaccination (41, 78, 79). Such interactions have not been studied within the tumor microenvironment, but this would be of significant interest given our data suggest that the expression of CXCL9 by host immune cells is critical for the therapeutic effect of immune checkpoint blockade.

In summary, our data indicate that the production of CXCR3 ligands is critical for the therapeutic effect of dual anti-PD-1/anti-CTLA-4 therapy and identifies macrophages as the predominant source of CXCL9 both in preclinical models and in patients treated with immunotherapy. These cells were predicative of response to immune checkpoint blockade and thus novel strategies to enhance CXCL9/10 production, particularly by macrophages, have the potential to enhance the efficacy of immunotherapy in patients.

Disclosure of Potential Conflicts of Interest

P. Savas is an advisory board member/unpaid consultant for Genentech. R.A. Scolyer reports receiving speakers bureau honoraria from Bristol-Myers Squibb, and is an advisory board member/unpaid consultant for Merck Sharp & Dohme, Novartis, Myriad, MeraCare, and Amgen. G.V. Long is an employee/paid consultant for Aduro, Amgen, Array, Bristol-Myers Squibb, Merck Sharpe & Dohme, Novartis, Oncosec, Pierre Fabre, and Roche. S. Loi is an employee/paid consultant for Aduro Biotech, reports receiving commercial research grants to her institution from Novartis, Bristol-Myers Squibb, Merck, Roche-Genentech, Puma Biotechnology and Eli Lilly, and is an advisory board member/unpaid consultant for Seattle Genetics, Pfizer, Novartis, Bristol-Myers Squibb, Merck, AstraZeneca, and Roche-Genentech. No potential conflicts of interest were disclosed by the other authors.

Published OnlineFirst October 21, 2019; DOI: 10.1158/1078-0432.CCR-19-1868

Authors' Contributions

Conception and design: I.G. House, P.K. Darcy, P.A. Beavis
Development of methodology: I.G. House, J. Lai, A.J. Oliver, S. Loi, P.A. Beavis
Acquisition of data (provided animals, acquired and managed patients, provided facilities, etc.): I.G. House, P. Savas, J. Lai, A.X.Y. Chen, Z.L. Teo, K.L. Todd, M.A. Henderson, L. Giuffrida, E.V. Petley, T.N. Gide, G.V. Long, J.S. Wilmott, S. Loi, P.K. Darcy, P.A. Beavis
Analysis and interpretation of data (e.g., statistical analysis, biostatistics, computational analysis): I.G. House, P. Savas, J. Lai, A.J. Oliver, Z.L. Teo, K. Sek, C. Quek, R.A. Scolyer, J.S. Wilmott, S. Loi, P.K. Darcy, P.A. Beavis
Writing, review, and/or revision of the manuscript: I.G. House, P. Savas, J. Lai, A.J. Oliver, Z.L. Teo, M.A. Henderson, L. Giuffrida, K. Sek, S. Mardiana, R.A. Scolyer, G.V. Long, J.S. Wilmott, S. Loi, P.K. Darcy, P.A. Beavis
Administrative, technical, or material support (i.e., reporting or organizing data, constructing databases): I.G. House, L. Giuffrida, P.K. Darcy
Study supervision: P.K. Darcy, P.A. Beavis

Acknowledgments

The authors would like to acknowledge the assistance of the Animal Facility technicians at the Peter MacCallum Cancer Centre. This work was funded by a Program Grant from the National Health and Medical Research Council (NHMRC; grant number 1132373) and a National Breast Cancer Foundation Grant (IIRS-19-016 19-22). P.A. Beavis is supported by National Breast Cancer Foundation Fellowship (ID# ECF-17-005). P.K. Darcy is supported by an NHMRC Senior Research Fellowship (APP1136680).

The costs of publication of this article were defrayed in part by the payment of page charges. This article must therefore be hereby marked *advertisement* in accordance with 18 U.S.C. Section 1734 solely to indicate this fact.

Received June 16, 2019; revised September 11, 2019; accepted October 9, 2019; published first October 21, 2019.

References

1. Ribas A, Wolchok JD. Cancer immunotherapy using checkpoint blockade. Science 2018;359:1350–5.
2. Sharma P, Allison JP. Immune checkpoint targeting in cancer therapy: toward combination strategies with curative potential. Cell 2015;161:205–14.
3. Rizvi NA, Hellmann MD, Snyder A, Kvistborg P, Makarov V, Havel JJ, et al. Cancer immunology. mutational landscape determines sensitivity to PD-1 blockade in non-small cell lung cancer. Science 2015;348:124–8.
4. Tumeh PC, Harview CL, Yearley JH, Shintaku IP, Taylor EJ, Robert L, et al. PD-1 blockade induces responses by inhibiting adaptive immune resistance. Nature 2014;515:568–71.
5. Gajewski TF, Corrales L, Williams J, Horton B, Sivan A, Spranger S, et al. Cancer immunotherapy targets based on understanding the T cell-inflamed versus non-T cell-inflamed tumor microenvironment. Adv Exp Med Biol 2017;1036:19–31.
6. Denkert C, von Minckwitz G, Brase JC, Sinn BV, Gade S, Kronenwett R, et al. Tumor-infiltrating lymphocytes and response to neoadjuvant chemotherapy with or without carboplatin in human epidermal growth factor receptor 2-positive and triple-negative primary breast cancers. J Clin Oncol 2015;33:983–91.
7. Ding Q, Lu P, Xia Y, Ding S, Fan Y, Li X, et al. CXCL9: evidence and contradictions for its role in tumor progression. Cancer Med 2016;5:3246–59.
8. Zumwalt TJ, Arnold M, Goel A, Boland CR. Active secretion of CXCL10 and CCL5 from colorectal cancer microenvironments associates with GranzymeB+ CD8+ T-cell infiltration. Oncotarget 2015;6:2981–91.
9. de Mingo Pulido A, Gardner A, Hiebler S, Soliman H, Rugo HS, Krummel MF, et al. TIM-3 regulates CD103(+) dendritic cell function and response to chemotherapy in breast cancer. Cancer Cell 2018;33:60–74.
10. Hong M, Puaux AL, Huang C, Loumagne L, Tow C, Mackay C, et al. Chemotherapy induces intratumoral expression of chemokines in cutaneous melanoma, favoring T-cell infiltration and tumor control. Cancer Res 2011;71:6997–7009.
11. Specht K, Harbeck N, Smida J, Annecke K, Reich U, Naehrig J, et al. Expression profiling identifies genes that predict recurrence of breast cancer after adjuvant CMF-based chemotherapy. Breast Cancer Res Treat 2009;118:45–56.
12. Spranger S, Dai D, Horton B, Gajewski TF. Tumor-residing Batf3 dendritic cells are required for effector T cell trafficking and adoptive T cell therapy. Cancer Cell 2017;31:711–23.
13. Tokunaga R, Zhang W, Naseem M, Puccini A, Berger MD, Soni S, et al. CXCL9, CXCL10, CXCL11/CXCR3 axis for immune activation - a target for novel cancer therapy. Cancer Treat Rev 2018;63:40–7.
14. Bedognetti D, Spivey TL, Zhao Y, Uccellini L, Tomei S, Dudley ME, et al. CXCR3/CCR5 pathways in metastatic melanoma patients treated with adoptive therapy and interleukin-2. Br J Cancer 2013;109:2412–23.
15. Weng Y, Siciliano SJ, Waldburger KE, Sirotina-Meisher A, Staruch MJ, Daugherty BL, et al. Binding and functional properties of recombinant and endogenous CXCR3 chemokine receptors. J Biol Chem 1998;273:18288–91.
16. Cole KE, Strick CA, Paradis TJ, Ogborne KT, Loetscher M, Gladue RP, et al. Interferon-inducible T cell alpha chemoattractant (I-TAC): a novel non-ELR CXC chemokine with potent activity on activated T cells through selective high affinity binding to CXCR3. J Exp Med 1998;187:2009–21.
17. Colvin RA, Campanella GS, Sun J, Luster AD. Intracellular domains of CXCR3 that mediate CXCL9, CXCL10, and CXCL11 function. J Biol Chem 2004;279:30219–27.
18. Metzemaekers M, Vanheule V, Janssens R, Struyf S, Proost P. Overview of the mechanisms that may contribute to the non-redundant activities of interferon-inducible CXC chemokine receptor 3 ligands. Front Immunol 2017;8:1970.
19. Beavis PA, Henderson MA, Giuffrida L, Davenport AJ, Petley EV, House IG, et al. Dual PD-1 and CTLA-4 checkpoint blockade promotes antitumor immune responses through CD4(+)Foxp3(-) cell-mediated modulation of CD103(+) dendritic cells. Cancer Immunol Res 2018;6:1069–81.
20. Ritchie ME, Phipson B, Wu D, Hu Y, Law CW, Shi W, et al. limma powers differential expression analyses for RNA-sequencing and microarray studies. Nucleic Acids Res 2015;43:e47.
21. Robinson MD, Oshlack A. A scaling normalization method for differential expression analysis of RNA-seq data. Genome Biol 2010;11:R25.
22. Law CW, Chen Y, Shi W, Smyth GK. Voom: precision weights unlock linear model analysis tools for RNA-seq read counts. Genome Biol 2014;15:R29.
23. Gide TN, Quek C, Menzies AM, Tasker AT, Shang P, Holst J, et al. Distinct immune cell populations define response to anti-PD-1 monotherapy and anti-PD-1/anti-CTLA-4 combined therapy. Cancer Cell 2019;35:238–55.
24. Mariathasan S, Turley SJ, Nickles D, Castiglioni A, Yuen K, Wang Y, et al. TGFbeta attenuates tumour response to PD-L1 blockade by contributing to exclusion of T cells. Nature 2018;554:544–8.
25. Wu D, Smyth GK. Camera: a competitive gene set test accounting for inter-gene correlation. Nucleic Acids Res 2012;40:e133.
26. Subramanian A, Tamayo P, Mootha VK, Mukherjee S, Ebert BL, Gillette MA, et al. Gene set enrichment analysis: a knowledge-based approach for interpreting genome-wide expression profiles. Proc Natl Acad Sci U S A 2005;102:15545–50.
27. Riaz N, Havel JJ, Makarov V, Desrichard A, Urba WJ, Sims JS, et al. Tumor and microenvironment evolution during immunotherapy with nivolumab. Cell 2017;171:934–49.
28. Jiang P, Gu S, Pan D, Fu J, Sahu A, Hu X, et al. Signatures of T cell dysfunction and exclusion predict cancer immunotherapy response. Nat Med 2018;24:1550–8.
29. Sade-Feldman M, Yizhak K, Bjorgaard SL, Ray JP, de Boer CG, Jenkins RW, et al. Defining T cell states associated with response to checkpoint immunotherapy in melanoma. Cell 2018;175:998–1013.
30. Jerby-Arnon L, Shah P, Cuoco MS, Rodman C, Su MJ, Melms JC, et al. A cancer cell program promotes T cell exclusion and resistance to checkpoint blockade. Cell 2018;175:984–97.

31. Puram SV, Tirosh I, Parikh AS, Patel AP, Yizhak K, Gillespie S, et al. Single-cell transcriptomic analysis of primary and metastatic tumor ecosystems in head and neck cancer. Cell 2017;171:1611–24.
32. Zilionis R, Engblom C, Pfirschke C, Savova V, Zemmour D, Saatcioglu HD, et al. Single-cell transcriptomics of human and mouse lung cancers reveals conserved myeloid populations across individuals and species. Immunity 2019;50:1317–34.
33. Butler A, Hoffman P, Smibert P, Papalexi E, Satija R. Integrating single-cell transcriptomic data across different conditions, technologies, and species. Nat Biotechnol 2018;36:411–20.
34. Finak G, McDavid A, Yajima M, Deng J, Gersuk V, Shalek AK, et al. MAST: a flexible statistical framework for assessing transcriptional changes and characterizing heterogeneity in single-cell RNA sequencing data. Genome Biol 2015;16:278.
35. Kumar MP, Du J, Lagoudas G, Jiao Y, Sawyer A, Drummond DC, et al. Analysis of single-cell RNA-Seq identifies cell-cell communication associated with tumor characteristics. Cell Rep 2018;25:1458–68.
36. Rueda OM, Sammut SJ, Seoane JA, Chin SF, Caswell-Jin JL, Callari M, et al. Dynamics of breast-cancer relapse reveal late-recurring ER-positive genomic subgroups. Nature 2019;567:399–404.
37. Liu J, Lichtenberg T, Hoadley KA, Poisson LM, Lazar AJ, Cherniack AD, et al. An integrated TCGA Pan-Cancer Clinical Data Resource to drive high-quality survival outcome analytics. Cell 2018;173:400–16.
38. Curran MA, Montalvo W, Yagita H, Allison JP. PD-1 and CTLA-4 combination blockade expands infiltrating T cells and reduces regulatory T and myeloid cells within B16 melanoma tumors. Proc Natl Acad Sci U S A 2010;107:4275–80.
39. Boutros C, Tarhini A, Routier E, Lambotte O, Ladurie FL, Carbonnel F, et al. Safety profiles of anti-CTLA-4 and anti-PD-1 antibodies alone and in combination. Nat Rev Clin Oncol 2016;13:473–86.
40. Twyman-Saint Victor C, Rech AJ, Maity A, Rengan R, Pauken KE, Stelekati E, et al. Radiation and dual checkpoint blockade activate non-redundant immune mechanisms in cancer. Nature 2015;520:373–7.
41. Groom JR, Richmond J, Murooka TT, Sorensen EW, Sung JH, Bankert K, et al. CXCR3 chemokine receptor-ligand interactions in the lymph node optimize CD4+ T helper 1 cell differentiation. Immunity 2012;37:1091–103.
42. Guirnalda P, Wood L, Goenka R, Crespo J, Paterson P. Interferon gamma-induced intratumoral expression of CXCL9 alters the local distribution of T cells following immunotherapy with Listeria monocytogenes. Oncoimmunology 2013;2:e25752.
43. Binnewies M, Roberts EW, Kersten K, Chan V, Fearon DF, Merad M, et al. Understanding the tumor immune microenvironment (TIME) for effective therapy. Nat Med 2018;24:541–50.
44. van der Woude LL, Gorris MAJ, Halilovic A, Figdor CG, de Vries IJM. Migrating into the tumor: a roadmap for T cells. Trends Cancer 2017;3:797–808.
45. Nywening TM, Belt BA, Cullinan DR, Panni RZ, Han BJ, Sanford DE, et al. Targeting both tumour-associated CXCR2(+) neutrophils and CCR2(+) macrophages disrupts myeloid recruitment and improves chemotherapeutic responses in pancreatic ductal adenocarcinoma. Gut 2018;67:1112–23.
46. Li J, Byrne KT, Yan F, Yamazoe T, Chen Z, Baslan T, et al. Tumor cell-intrinsic factors underlie heterogeneity of immune cell infiltration and response to immunotherapy. Immunity 2018;49:178–93.
47. Gorbachev AV, Kobayashi H, Kudo D, Tannenbaum CS, Finke JH, Shu S, et al. CXC chemokine ligand 9/monokine induced by IFN-gamma production by tumor cells is critical for T cell-mediated suppression of cutaneous tumors. J Immunol 2007;178:2278–86.
48. Zhang R, Tian L, Chen LJ, Xiao F, Hou JM, Zhao X, et al. Combination of MIG (CXCL9) chemokine gene therapy with low-dose cisplatin improves therapeutic efficacy against murine carcinoma. Gene Ther 2006;13:1263–71.
49. Hannesdottir L, Tymoszuk P, Parajuli N, Wasmer MH, Philipp S, Daschil N, et al. Lapatinib and doxorubicin enhance the Stat1-dependent antitumor immune response. Eur J Immunol 2013;43:2718–29.
50. Pan J, Burdick MD, Belperio JA, Xue YY, Gerard C, Sharma S, et al. CXCR3/CXCR3 ligand biological axis impairs RENCA tumor growth by a mechanism of immunoangiostasis. J Immunol 2006;176:1456–64.
51. Reckamp KL, Figlin RA, Moldawer N, Pantuck AJ, Belldegrun AS, Burdick MD, et al. Expression of CXCR3 on mononuclear cells and CXCR3 ligands in patients with metastatic renal cell carcinoma in response to systemic IL-2 therapy. J Immunother 2007;30:417–24.
52. Wang X, Zhang FC, Zhao HY, Lu XL, Sun Y, Xiong ZY, et al. Human IP10-scFv and DC-induced CTL synergistically inhibit the growth of glioma in a xenograft model. Tumour Biol 2014;35:7781–91.
53. Mikucki ME, Fisher DT, Matsuzaki J, Skitzki JJ, Gaulin NB, Muhitch JB, et al. Non-redundant requirement for CXCR3 signalling during tumoricidal T-cell trafficking across tumour vascular checkpoints. Nat Commun 2015;6:7458.
54. Li J, Ybarra R, Mak J, Herault A, De Almeida P, Arrazate A, et al. IFNγ-induced chemokines are required for CXCR3-mediated T-cell recruitment and antitumor efficacy of anti-HER2/CD3 bispecific antibody. Clin Cancer Res 2018;24:6447–58.
55. Chheda ZS, Sharma RK, Jala VR, Luster AD, Haribabu B. Chemoattractant receptors BLT1 and CXCR3 regulate antitumor immunity by facilitating CD8+ T cell migration into tumors. J Immunol 2016;197:2016–26.
56. Dangaj D, Bruand M, Grimm AJ, Ronet C, Barras D, Duttagupta PA, et al. Cooperation between constitutive and inducible chemokines enables T cell engraftment and immune attack in solid tumors. Cancer Cell 2019;35:885–900.
57. Zhang S, Zhong M, Wang C, Xu Y, Gao WQ, Zhang Y, et al. CCL5-deficiency enhances intratumoral infiltration of CD8(+) T cells in colorectal cancer. Cell Death Dis 2018;9:766.
58. Ban Y, Mai J, Li X, Mitchell-Flack M, Zhang T, Zhang L, et al. Targeting autocrine CCL5-CCR5 axis reprograms immunosuppressive myeloid cells and reinvigorates antitumor immunity. Cancer Res 2017;77:2857–68.
59. Savas P, Virassamy B, Ye C, Salim A, Mintoff CP, Caramia F, et al. Single-cell profiling of breast cancer T cells reveals a tissue-resident memory subset associated with improved prognosis. Nat Med 2018;24:986–93.
60. Ji RR, Chasalow SD, Wang L, Hamid O, Schmidt H, Cogswell J, et al. An immune-active tumor microenvironment favors clinical response to ipilimumab. Cancer Immunol Immunother 2012;61:1019–31.
61. Barreira da Silva R, Laird ME, Yatim N, Fiette L, Ingersoll MA, Albert ML, et al. Dipeptidylpeptidase 4 inhibition enhances lymphocyte trafficking, improving both naturally occurring tumor immunity and immunotherapy. Nat Immunol 2015;16:850–8.
62. Decalf J, Tarbell KV, Casrouge A, Price JD, Linder G, Mottez E, et al. Inhibition of DPP4 activity in humans establishes its *in vivo* role in CXCL10 post-translational modification: prospective placebo-controlled clinical studies. EMBO Mol Med 2016;8:679–83.
63. Li Y, Fang M, Zhang J, Wang J, Song Y, Shi J, et al. Hydrogel dual delivered celecoxib and anti-PD-1 synergistically improve antitumor immunity. Oncoimmunology 2015;5:e1074374.
64. Peng D, Kryczek I, Nagarsheth N, Zhao L, Wei S, Wang W, et al. Epigenetic silencing of TH1-type chemokines shapes tumour immunity and immunotherapy. Nature 2015;527:249–53.
65. Wendel M, Galani IE, Suri-Payer E, Cerwenka A. Natural killer cell accumulation in tumors is dependent on IFN-gamma and CXCR3 ligands. Cancer Res 2008;68:8437–45.
66. Hirako IC, Ataide MA, Faustino L, Assis PA, Sorensen EW, Ueta H, et al. Splenic differentiation and emergence of CCR5(+)CXCL9(+)CXCL10(+) monocyte-derived dendritic cells in the brain during cerebral malaria. Nat Commun 2016;7:13277.
67. Peng W, Liu C, Xu C, Lou Y, Chen J, Yang Y, et al. PD-1 blockade enhances T-cell migration to tumors by elevating IFN-gamma inducible chemokines. Cancer Res 2012;72:5209–18.
68. Bronger H, Kraeft S, Schwarz-Boeger U, Cerny C, Stöckel A, Avril S, et al. Modulation of CXCR3 ligand secretion by prostaglandin E2 and cyclooxygenase inhibitors in human breast cancer. Breast Cancer Res 2012;14:R30.
69. Chow MT, Ozga AJ, Servis RL, Frederick DT, Lo JA, Fisher DE, et al. Intratumoral activity of the CXCR3 chemokine system is required for the efficacy of anti-PD-1 therapy. Immunity 2019;50:1498–512.
70. Yost KE, Satpathy AT, Wells DK, Qi Y, Wang C, Kageyama R, et al. Clonal replacement of tumor-specific T cells following PD-1 blockade. Nat Med 2019;25:1251–9.
71. Ohmori Y, Schreiber RD, Hamilton TA. Synergy between interferon-gamma and tumor necrosis factor-alpha in transcriptional activation is mediated by cooperation between signal transducer and activator of transcription 1 and nuclear factor kappaB. J Biol Chem 1997;272:14899–907.

Published OnlineFirst October 21, 2019; DOI: 10.1158/1078-0432.CCR-19-1868

72. Clarke DL, Clifford RL, Jindarat S, Proud D, Pang L, Belvisi M, et al. TNFα and IFNγ synergistically enhance transcriptional activation of CXCL10 in human airway smooth muscle cells via STAT-1, NF-κB, and the transcriptional coactivator CREB-binding protein. J Biol Chem 2010;285: 29101–10.
73. Zaretsky JM, Garcia-Diaz A, Shin DS, Escuin-Ordinas H, Hugo W, Hu-Lieskovan S, et al. Mutations associated with acquired resistance to PD-1 blockade in melanoma. N Engl J Med 2016;375:819–29.
74. Shin DS, Zaretsky JM, Escuin-Ordinas H, Garcia-Diaz A, Hu-Lieskovan S, Kalbasi A, et al. Primary resistance to PD-1 blockade mediated by JAK1/2 mutations. Cancer Discov 2017;7:188–201.
75. Manguso RT, Pope HW, Zimmer MD, Brown FD, Yates KB, Miller BC, et al. In vivo CRISPR screening identifies Ptpn2 as a cancer immunotherapy target. Nature 2017;547:413–8.
76. Kearney CJ, Vervoort SJ, Hogg SJ, Ramsbottom KM, Freeman AJ, Lalaoui N, et al. Tumor immune evasion arises through loss of TNF sensitivity. Sci Immunol 2018;3. doi: 10.1126/sciimmunol.aar3451.
77. Meiser A, Mueller A, Wise EL, McDonagh EM, Petit SJ, Saran N, et al. The chemokine receptor CXCR3 is degraded following internalization and is replenished at the cell surface by de novo synthesis of receptor. J Immunol 2008;180: 6713–24.
78. Woodruff MC, Heesters BA, Herndon CN, Groom JR, Thomas PG, Luster AD, et al. Trans-nodal migration of resident dendritic cells into medullary interfollicular regions initiates immunity to influenza vaccine. J Exp Med 2014;211: 1611–21.
79. Lian J, Luster AD. Chemokine-guided cell positioning in the lymph node orchestrates the generation of adaptive immune responses. Curr Opin Cell Biol 2015;36:1–6.

Published OnlineFirst October 21, 2019; DOI: 10.1158/1078-0432.CCR-19-1868

Clinical Cancer Research

Macrophage-Derived CXCL9 and CXCL10 Are Required for Antitumor Immune Responses Following Immune Checkpoint Blockade

Imran G. House, Peter Savas, Junyun Lai, et al.

Clin Cancer Res 2020;26:487-504. Published OnlineFirst October 21, 2019.